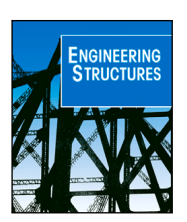
ELSEVIER

Contents lists available at ScienceDirect

Engineering Structures

journal homepage: www.elsevier.com/locate/engstruct





Isogeometric model reconstruction of open shells via Ricci flow and quadrilateral layout-inducing energies

Kendrick M. Shepherd a,*, Xianfeng David Gu^b, Thomas J.R. Hughes ^c

- a Department of Civil and Construction Engineering, Brigham Young University, Engineering Building 430, Provo, UT, 84602-4081, USA
- b Department of Computer Science, Stony Brook University, New Computer Science Building, Stony Brook, NY, 11794-2424, USA
- c Oden Institute for Computational Engineering and Sciences, The University of Texas at Austin, 201 East 24th Street, C0200, Austin, TX, 78712-1229, USA

ARTICLE INFO

This paper is dedicated to Professor Herbert Mang in honor of his numerous scientific contributions, his long and dedicated service to the international engineering community, and in celebration of his 80th birthday in January 2022.

Keywords: Quadrilateral layout Global parameterization Spline reconstruction Trim Shell analysis Isogeometric analysis Computer-aided design

ABSTRACT

Isogeometric analysis has received extensive attention in the last decade, but despite its merits, many isogeometric models are still produced manually or semi-manually. In this work, we introduce a new technique using Ricci flow and a carefully constrained minimization to convert trimmed and faceted open geometries into watertight spline models free of trim and suitable for isogeometric analysis with potential for automation. This technique is used to rebuild parts of the US Army's DEVCOM Generic Hull vehicle and portions of a 1996 Dodge Neon finite element model into trim-free spline models. Isogeometric modal analysis is performed on each to show the viability of this reconstruction framework in generating IGA-suitable splines for shell analysis

1. Introduction

Engineering shell structural analysis requires an integrated designthrough-analysis framework. Under the current paradigm, a designer creates computer-aided design (CAD) geometry to define the intended shape by combining a set of smooth B-spline or NURBS patches into a so-called "boundary representation" or "B-Rep" (which may simply be a midsurface, or "open" B-Rep); an analyst then replaces it with a finite element mesh that only approximates the original CAD geometry. Not only is the precise geometry of the model lost in this procedure (which alone may have significant implications [1]), but underlying physics of the analysis may also be lost. Additionally, this process takes a significant amount of time (over 70% of the design-throughanalysis process) [2,3] and money [4]. Regarding the analysis of these faceted meshes, traditional finite element techniques for shells struggle with locking (which is alleviated by increasing polynomial degree [5]) and numerically-induced large spurious eigenvalues (which increase with increased polynomial degree [6]). For operations such as explicit dynamics, where the maximal time step is inversely proportional to the square root of the maximum eigenvalue [7, p. 335], increasing polynomial degree leads to a reduction of time step size and a concomitant increase in computational effort.

Isogeometric analysis (IGA), proposed in [8], aims to address these issues by using the same smooth basis functions employed in CAD for engineering analysis. Isogeometric techniques can be used to directly solve (without resorting to mixed methods) high order PDEs like the Kirchhoff-Love shell formulation [9,10] and to represent physics using smooth spline functions [6,8]. Isogeometric methods are more accurate per degree of freedom than traditional finite element methods [11–13] and can operate directly on the B-spline and NURBS geometries created in CAD without the need for an auxiliary faceted mesh [8,14]. Furthermore, the smoothness of isogeometric basis functions alleviate modal "outliers" introduced with traditional finite element techniques [6,12, 15], and increasing basis function smoothness and polynomial degree accordingly reduces locking [16-19]. Isogeometric shells admit highaccuracy, high-sparsity quadrature routines unavailable for traditional shells [18]. And finally, isogeometric techniques offer the potential of a single model suitable for both engineering design and analysis, reducing the time and expense associated with meshing.

Unfortunately, CAD models are not simply curvilinearly mapped rectangles, as are the B-spline and NURBS patches from which they emanate. Rather, CAD technologies piece B-spline and NURBS patches

E-mail addresses: kendrick.m.shepherd@byu.edu (K.M. Shepherd), gu@cs.stonybrook.edu (X.D. Gu), hughes@oden.utexas.edu (T.J.R. Hughes).

^{*} Corresponding author.

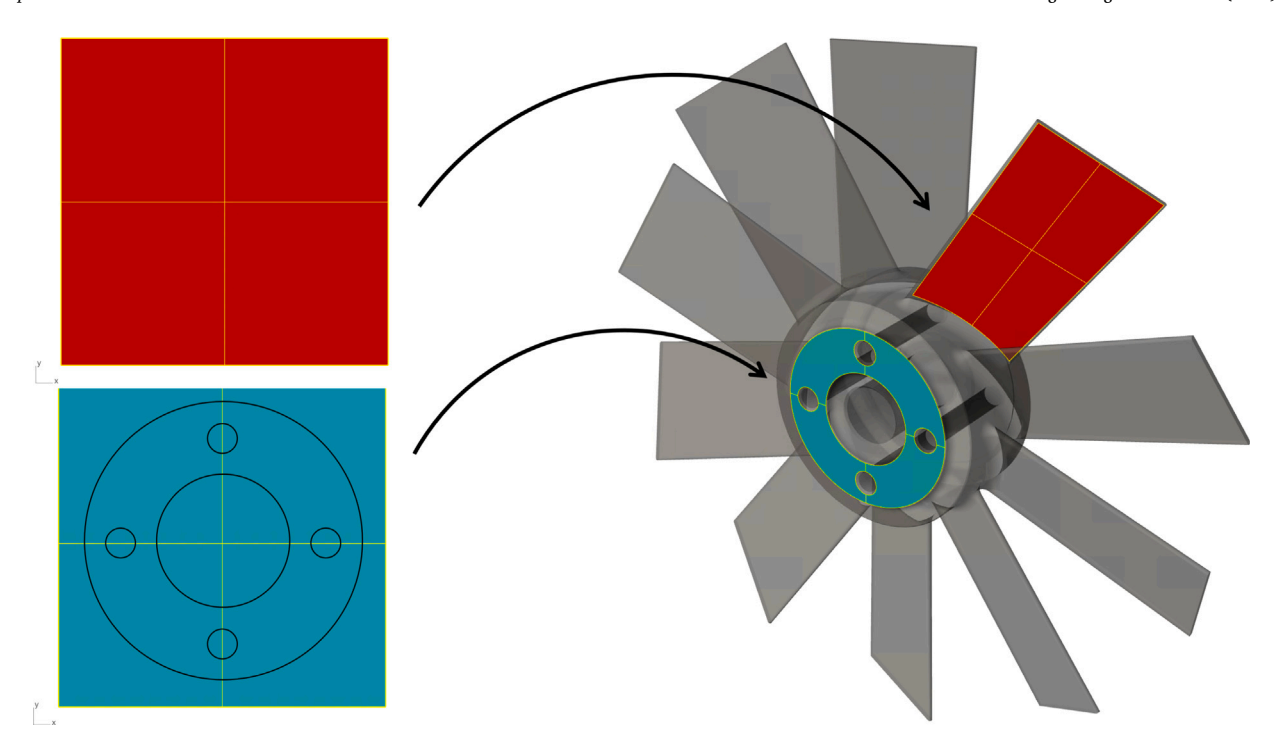


Fig. 1. A typical B-Rep geometry will consist of a topological gluing of multiple B-spline and NURBS tensor product patches mapped into a spatial configuration. In the presence of complicated topology or geometry, trimming operations—which mask portions of the tensor product spline—are ubiquitous. These trimming operations, though useful in rapid design prototyping, impede the use of the B-Rep in engineering analysis. This particular B-Rep is a sample engine turbine from Rolls Royce.

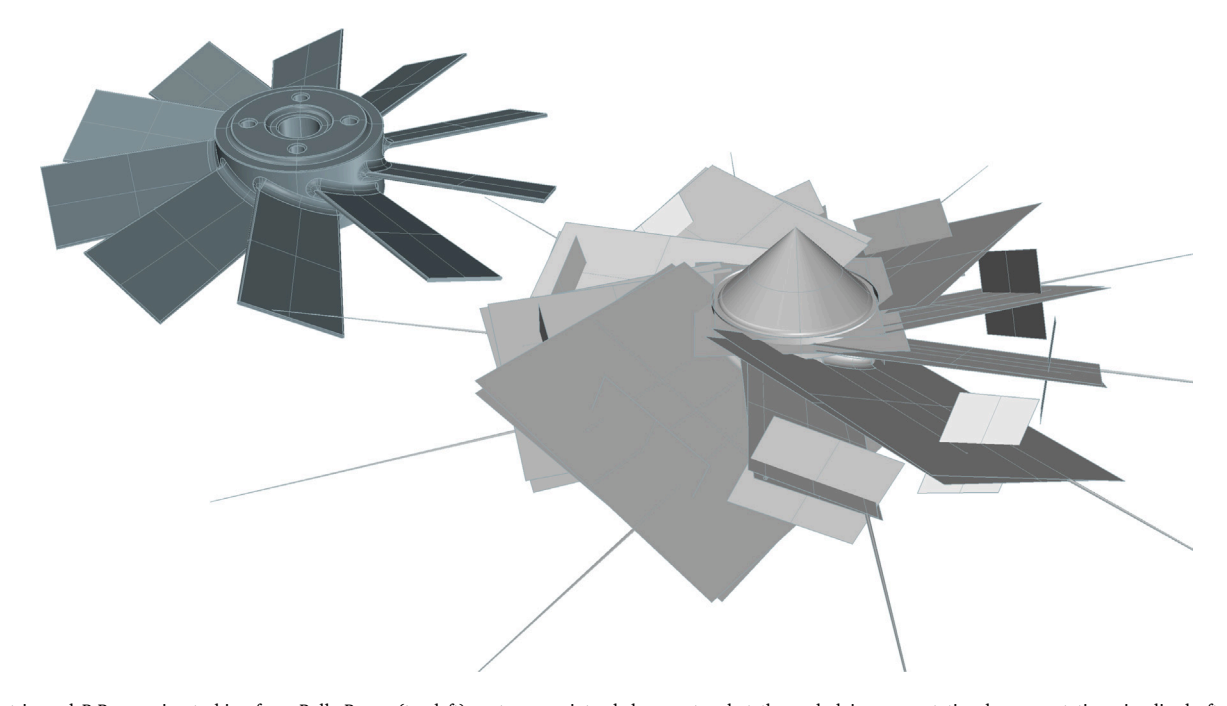


Fig. 2. A trimmed B-Rep engine turbine from Rolls Royce (top-left) portrays an intended geometry, but the underlying computational representation visualized after removing trimming features reveals that the model is defined by a complicated data structure bearing very little resemblance to the intended geometry.

together to define the boundary of an intended object, a computational representation called a B-Rep. Midsurfaces of these models, called open B-Reps, are created analogously. For models with complicated geometry or topology, Boolean operations are typically employed to portray the intended shape by masking unwanted parts of the underlying spline patches [20, p. 304–307], [21,22]. Aspects of this construction process are displayed in Fig. 1. Visually, the results portray the intended design, but these Boolean (a.k.a. "trimming") operations hide what is often a complex computer representation (see Fig. 2). Trimming breaks

spline function continuity [20, p. 305], [22], complicates numerical integration [23–25], and requires weak coupling of subdomains [26–29]. Because CAD software cannot exactly represent general trimming operations [30,31], approximations are made that lead to tiny gaps and overlaps between surface edges that should be coincident [22,32]. This leads to surfaces that are not "watertight". [22,32].

In this paper, we propose a new framework for converting open midsurface CAD geometries into isogeometric analysis-suitable, trimfree B-Reps using discrete surface Ricci flow and metric optimization.

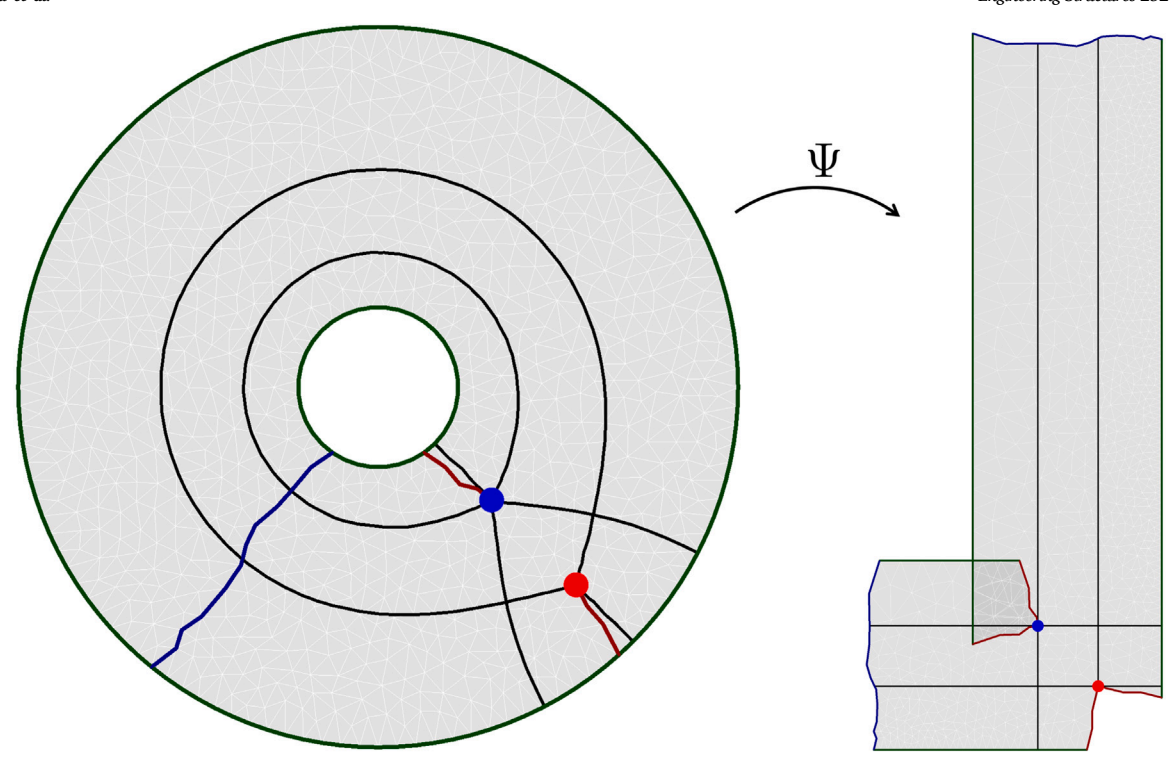


Fig. 3. A contrived quadrilateral layout on an annulus (left) is induced by a mapping of the cut annulus into the Euclidean plane (right). Here, the point in blue is a cone singularities of valence five and the point in red is a cone singularity of valence three. Cuts to cone singularities are given in red, while cuts to make the bracket a topological disk are in blue. Boundary curves are in dark green, while non-boundary integral curves are given in black. The coordinate differentials, du and dv, when traced from singular points and pulled back from the Euclidean plane to the original surface, integrate into curvilinear arcs partitioning the surface into a set of quadrilaterals. These differentials are depicted as black lines of constant u and v coordinates in the immersion, and curvilinear black arcs when pulled back to the original surface. (For interpretation of the references to color in this figure legend, the reader is referred to the web version of this article.)

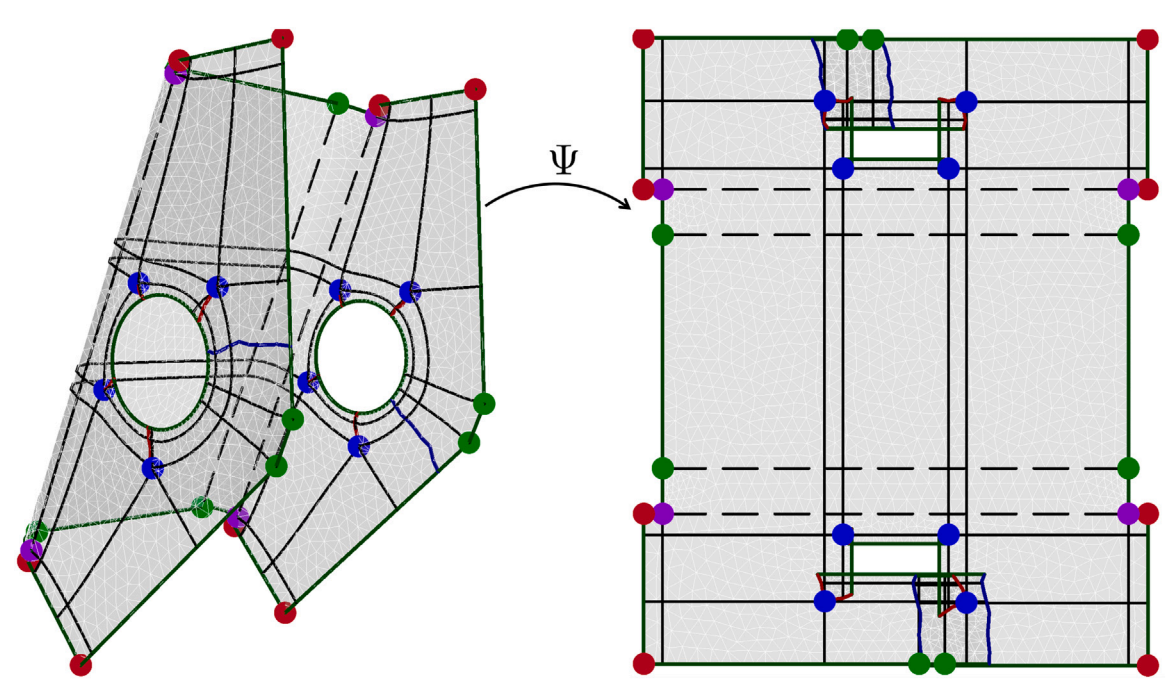


Fig. 4. A quadrilateral layout on a bracket of the DEVCOM Generic Hull vehicle (left) is induced by a mapping of the cut bracket into the Euclidean plane (right). Here, points in blue are cone singularities of index -1 (valence five), points in red are boundary cones of index 1, and points in purple are boundary cones of index -1. Feature points of the model that are not cone singularities in the defined parameterization are displayed in green. Cuts to cone singularities are given in red, while cuts to make the bracket a topological disk are in blue. Feature curves to be preserved in the computed layout are in dashed black. The coordinate differentials, du and dv, when traced from singular points and pulled back from the Euclidean plane to the original surface, integrate into curvilinear arcs partitioning the surface into a set of quadrilaterals. These differentials are depicted as black lines of constant u and v coordinates in the immersion, and curvilinear black arcs when pulled back to the original surface. (For interpretation of the references to color in this figure legend, the reader is referred to the web version of this article.)

In this framework, a trimmed CAD model is converted into an easy-to-compute, feature-aware surface triangulation with a topologically-constrained number of cone singularities (defined in Section 2). From

there, the discrete surface Ricci energy is minimized to determine a flat metric on the surface with cone singularities: this metric can be thought of as an immersion of a cut version of the surface into

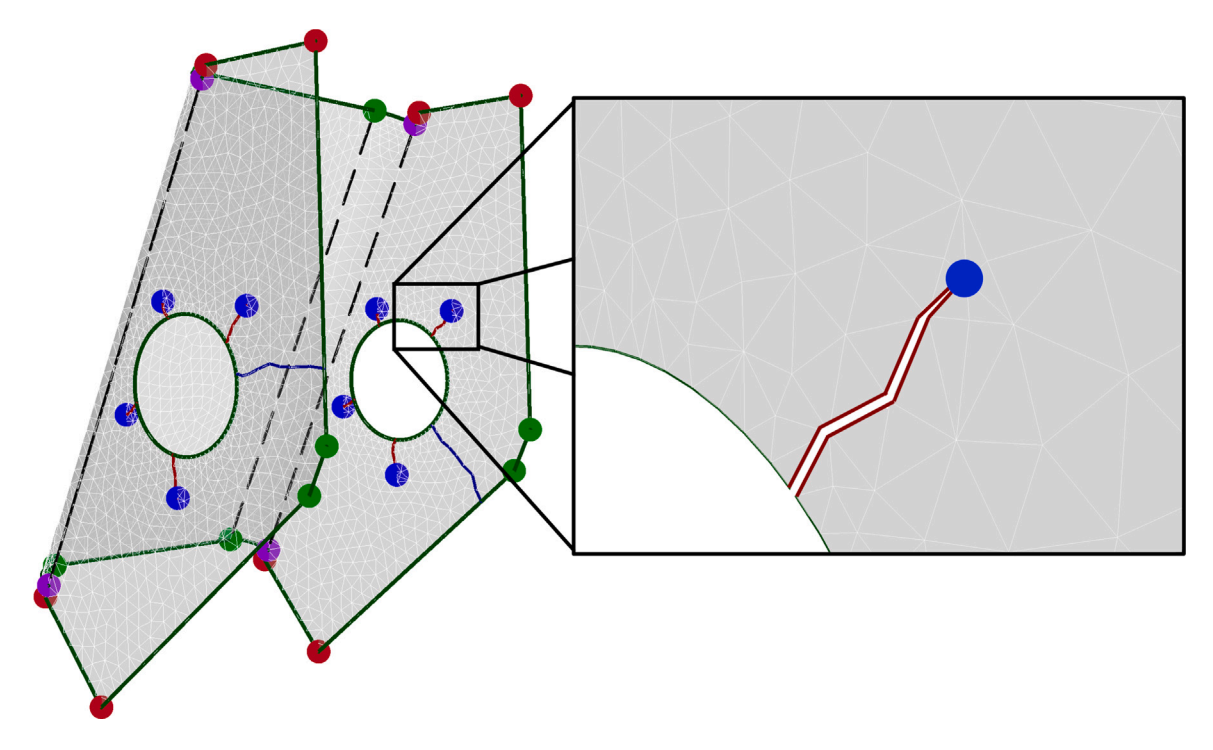


Fig. 5. A bracket with computed singular and feature points is cut into a topological disk. Singular points are shown in red, purple, and blue, with those in red and purple representing boundary cone singularities of index 1 and -1, respectively, and blue points representing interior cone singularities of index -1 (valence five). Points in green are features of the bracket that are not chosen to be cone singularities in the parameterization. Cuts to singularities are depicted in red, while cuts to make the bracket a topological disk are in blue. Curves in dark green and dashed black are the surface boundary and features, respectively. Notice that each singular point is either in the cutting graph or the surface boundary. Edges in the cutting graph are represented twice in the cut surface, vertices that are cut through are multiply represented, and vertices at the termination of the cutting graph are singly represented. (For interpretation of the references to color in this figure legend, the reader is referred to the web version of this article.)

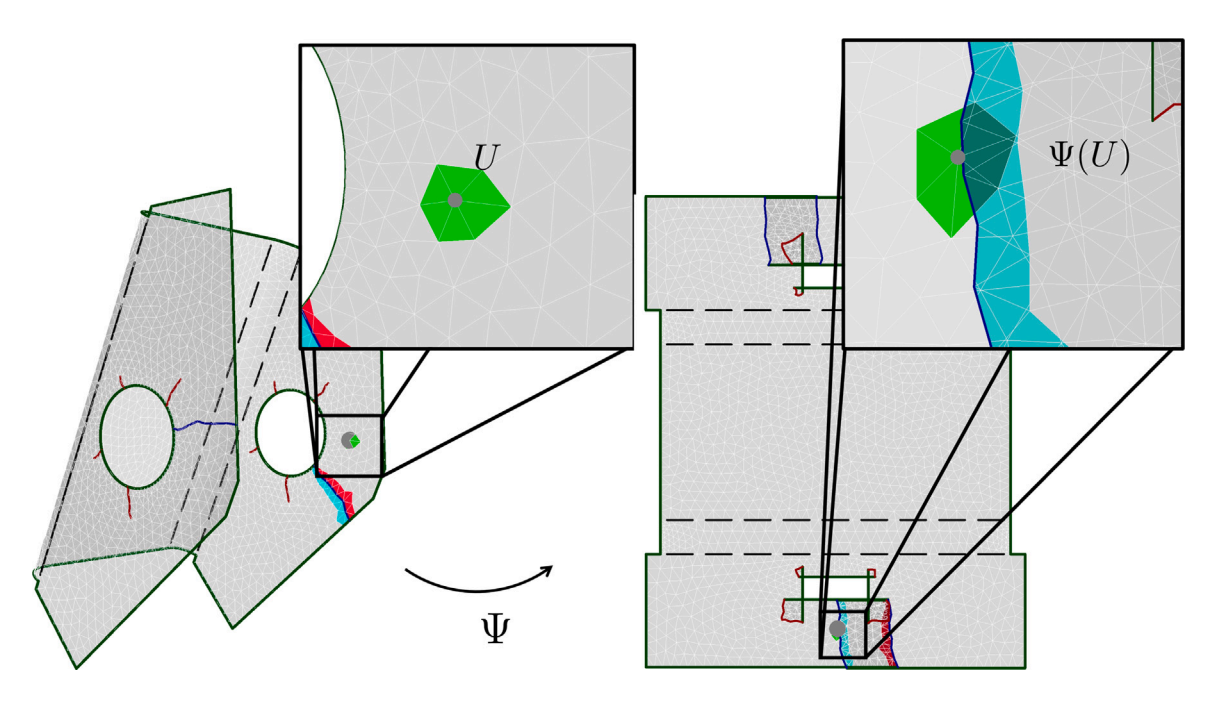


Fig. 6. A bracket of the DEVCOM Generic Hull vehicle is triangulated, and the neighborhood of one of its vertices is shown in green and subsequently mapped via a quad layout immersion map, Ψ . Additionally, all triangular faces on the sides of a particular homological cut are represented in either red or cyan and similarly mapped. Under the immersion, the image of the bracket is no longer injective: for example, the map takes portions of the vertex's neighborhood to the same coordinate locations that are part of the cyan side of the cut. However, an inverse is well-defined locally throughout the surface, including for each of these colored neighborhoods. (For interpretation of the references to color in this figure legend, the reader is referred to the web version of this article.)

the Euclidean plane, or a locally-bijective "parameterization". Subsequently, this parameterization is transformed into one that induces a quadrilateral layout on the surface. A quadrilateral layout can be thought of as a coarse quadrilateral partitioning of the surface that can

be refined as much as desired while still guaranteeing a valid quadrilateral refinement. Subsequently, the original CAD model is rebuilt using this computed layout as the skeleton for a set of quadrilateral watertight spline patches. Because this method employs a feature-aware

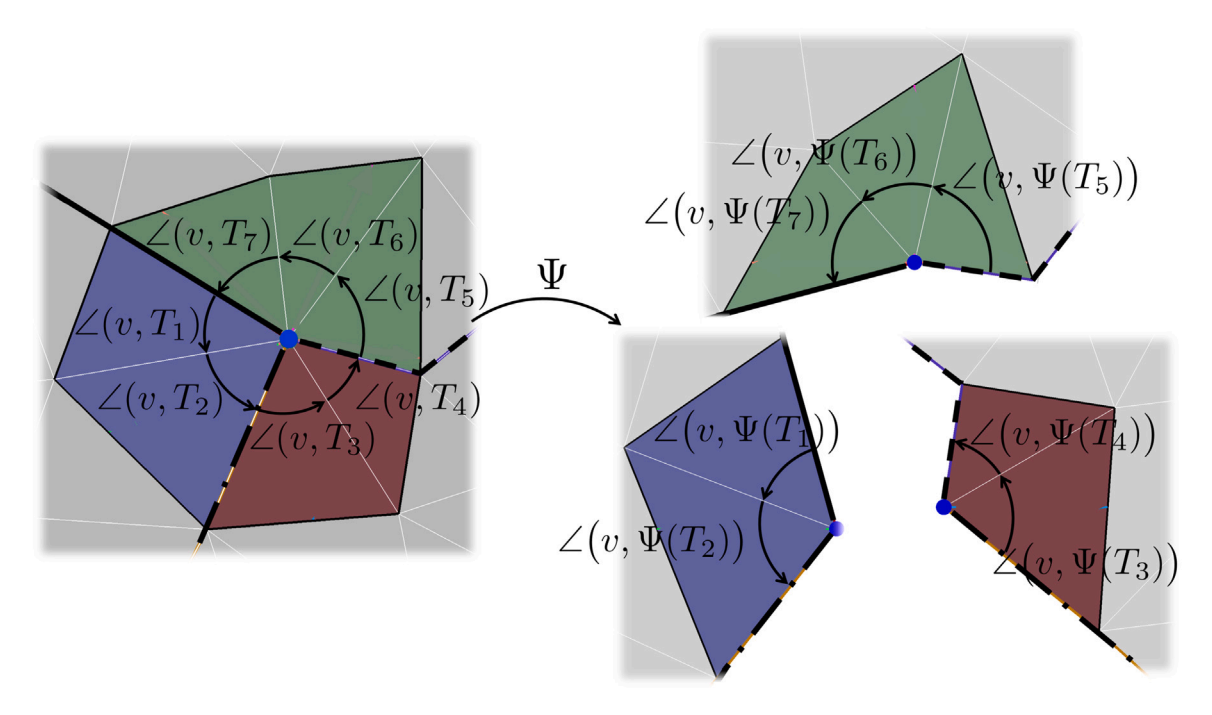


Fig. 7. The cutting graph of a surface—shown as a solid line, a dashed line, and a dash-dot line—splits this singular point into three child vertices. Accordingly, the neighborhood is split into three different portions, shown in blue, dark green, and dark magenta. Under the immersion mapping, the sum of the interior angles of this vertex with its incident triangles is $\frac{5\pi}{2}$, making the point a cone singularity of index -1 (i.e. valence five). (For interpretation of the references to color in this figure legend, the reader is referred to the web version of this article.)

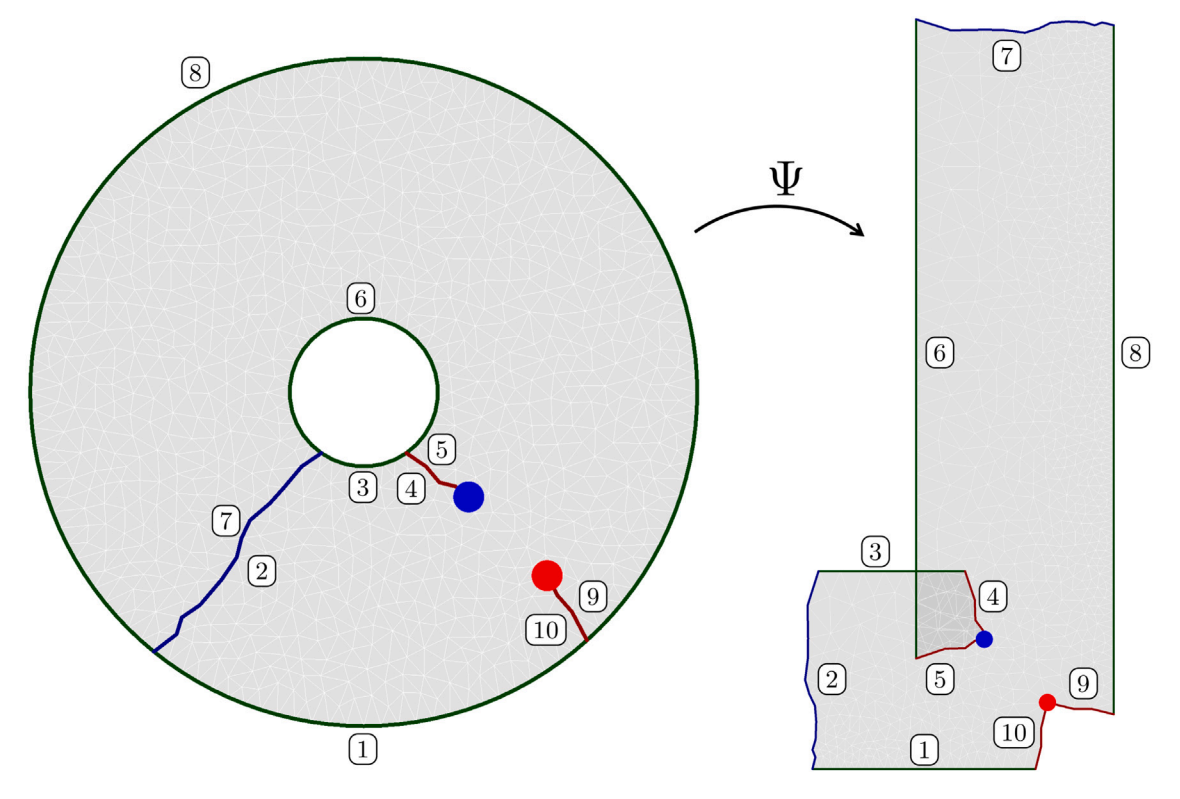


Fig. 8. A cut version of an annulus with a valence three (red) and a valence five (blue) singularity has subdomains of its boundary labeled. Because the cut surface is a topological disk, members of the cutting graph are also included. Under the quadrilateral layout inducing parameterization, Ψ , curves 1 and 3 are mapped to lines of constant v coordinate and curves 6 and 8 are mapped to lines of constant u coordinate. After a translation, curve 2 rotated by $\frac{\pi}{2}$ radians counter-clockwise (CCW) aligns with curve 7, and curve 4 matches curve 5 after rotation by $\frac{\pi}{2}$ radians CCW, and curve 9 matches curve 10 after rotation by $\frac{3\pi}{2}$ radians CCW. (For interpretation of the references to color in this figure legend, the reader is referred to the web version of this article.)

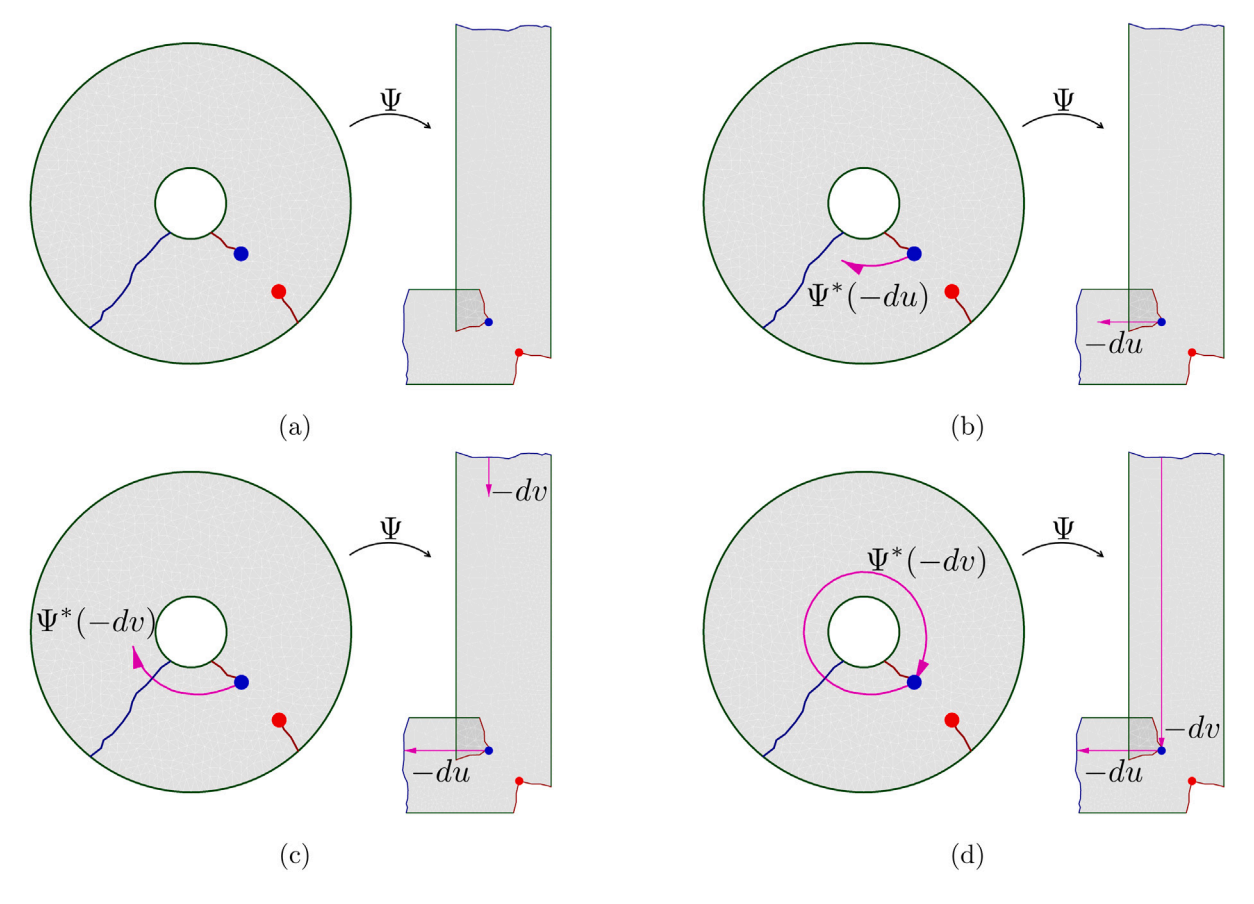


Fig. 9. An integral curve emanating from a singular curve in the -du coordinate direction is extracted (a line of constant v in the immersion). On the right of each subfigure is the integral curve under the quad layout immersion, Ψ , while on the left the integral curve of the pullback, Ψ^* , of the coordinate function differential into the spatial domain is shown. After reaching the cutting graph, the integral curve is continued in the -dv coordinate direction on the opposite side of the cut: the direction and location for continued integration is prescribed by Property Q4, and will generate a continuous curve in the spatial domain. This particular integral curve terminates when it returns to the singular point from which it began.

triangulation for the quadrilateral parameterization computation, it works equally-well in converting a faceted mesh into a feature-aware smooth spline surface.

1.1. Prior work

Two approaches have arisen to address the issues related to analysis of trimmed B-Rep models. The first, primarily driven by the analysis community, aims to address the issues of trimmed B-Reps by employing various generalizations of the classical cut cell method [23,25,29]. Here, cut elements are addressed using specialized integration techniques (see e.g. [23–25] and [36, p. 87–95]), numerical stabilization [37–40], and weak enforcement of both connectivity and boundary constraints [26–29]. This approach has seen significant progress of late [26,41,42], with recent works performing explicit dynamics computations on trimmed industrial B-Reps, [43], but additional efforts are still needed to ensure robustness in the presence of poorly shaped trimmed parametric spaces.

The other primary approach aiming to address analysis of trimmed CAD models seeks to rebuild a trimmed B-Rep prior to use in analysis. Many methods have been developed to rebuild a trimmed spline into a set of trim-free Bézier, B-spline, or NURBS patches by subdividing a trimmed patch's parametric domain into more regular shapes [32,45–47]. These techniques work well when the original model already meets high quality criteria, but generally cannot perform well on models for which the designer prescribed a poor parametric spline definition. Unfortunately, many models of engineering interest (including that of Fig. 2) may not meet the requisite quality criteria, and reconstruction using these techniques is difficult, and sometimes

impossible. Alternatively, recent works aim to redefine the B-Rep's underlying parametric domain by computing a global reparameterization using an auxiliary feature-aware surface triangulation [48–53]. Unlike typical analysis-suitable meshing methods that are predominantly well-structured quadrilaterals [54] and are labor-intensive to produce, the triangulations necessary for these reparameterizations can be unstructured and are easily-defined [55-57]. After computation of a quadrilateral-layout inducing reparameterization, splines are then fit to the computed layout. To date, many of these global reconstruction techniques have required significant user intervention [58,59], require expensive mixed-integer optimization [48,49,51,53,60], are limited by the use of templates [61,62] or certain types of singularities [63–65], or suffer from robustness issues [14]. Many are based on the frame field methods proposed in the computer graphics community [33,34,49,66, 67], which frequently employ mixed-integer optimization [48,49,51, 53] and require heuristics to address errors introduced by the nonintegrability of frame field vectors [53,67,68]. These methods generally cannot guarantee a locally-injective parameterization, meaning that some elements are either degenerate or possess non-positive Jacobian.

Global quadrilateral reparameterizations additionally require that defined cone singularities connect with each other through integral curves of the parameterization in order to segment the surface into a set of quadrilaterals. Traditionally, this has been done by forcing cone singularities to integer-valued coordinates using rounding [69], mixed integer optimization [48,49,68], or some other form of quantization [51,53,70]. The most recent methods in automating this process typically operate on a suitable global parameterization inducing a generalized T-mesh that is then transformed into a quadrilateral layout using either integer linear programming [53] or a simple linear

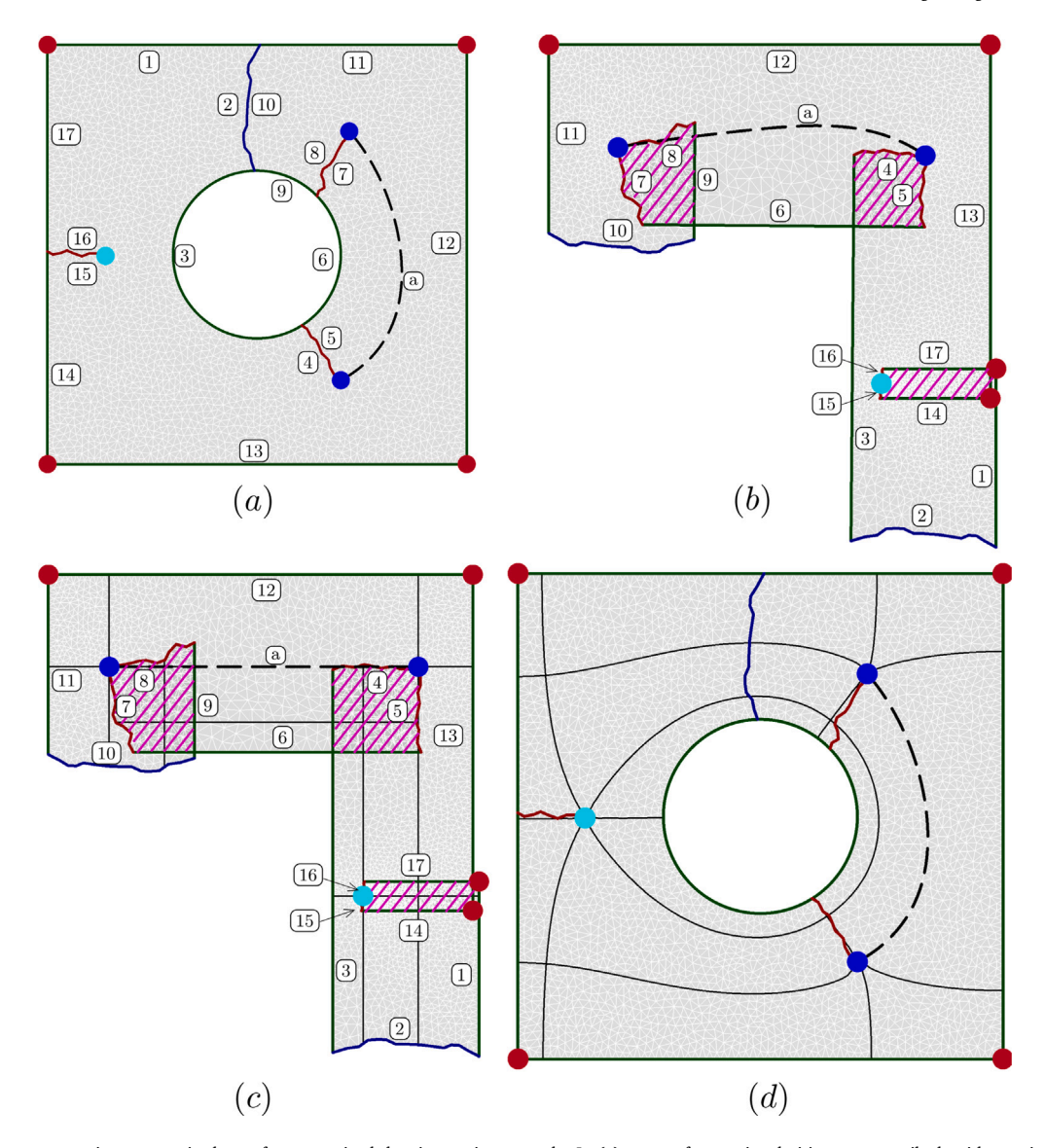


Fig. 10. The layout reconstruction process is shown for a contrived, but instructive example. In (a), a set of cone singularities are prescribed, with two interior cones of index -1 (valence 5), one interior cone of index -2 (valence 6), and four boundary cones of index 1. Cuts are made to each cone and to make the surface a topological disk, with edges of the disk labeled in clockwise manner; a feature curve is also shown as a dashed line and labeled using an "a". In (b), the surface is immersed into the plane based on the computation of discrete surface Ricci flow. This immersion does not induce a feature-aligned quadrilateral layout because the feature curve is not a line of constant u or v coordinate and because the boundary curves on the reentrant corners of the L-shaped immersion are also not lines of u or v coordinates. This parameterization is minimized against a quadrilateral layout-inducing energy to yield (c), an immersion that induces the quadrilateral layout of (d). In addition to the boundary curves and the feature curve "a", the black lines of (c) and (d) are integral curves from the singular points yielding the quadrilateral layout. Regions of magenta hatching are locations in which the immersion maps, though locally invertible, are not globally invertible. (For interpretation of the references to color in this figure legend, the reader is referred to the web version of this article.)

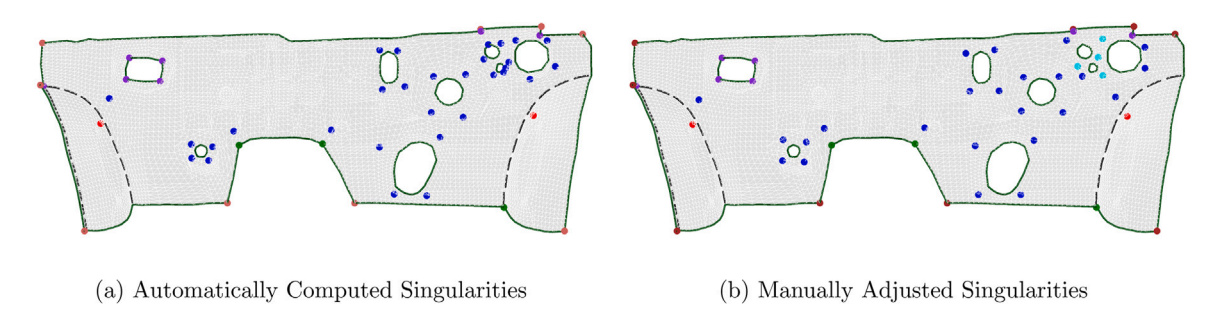


Fig. 11. On the left, singularities are automatically computed using [14], which combines the theory from [33,34]. Because of the high clustering of cone singularities in this configuration, singularities were manually modified to combine valence five singularities (blue) into valence six singularities (cyan) in the regions of high clustering (right). Note that the automatically-computed locations clarify potential positions for the manually-adjusted configuration. (For interpretation of the references to color in this figure legend, the reader is referred to the web version of this article.)

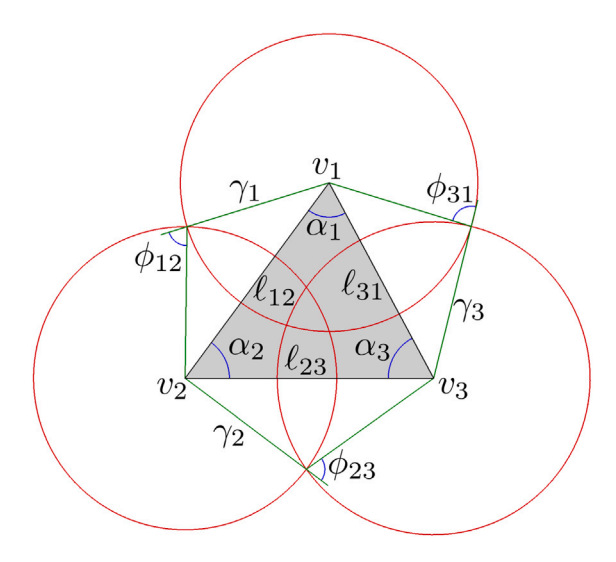


Fig. 12. After minimizing the discrete Ricci flow energy, the cut surface with flat metric can be isometrically immersed into the Euclidean plane using the law of cosines of Eq. (11) in conjunction with the lengths and angles depicted in this figure.

solve [70]. Quadrilateral layouts thus automatically extracted may still have poor connectivity properties, and additional methods have been proposed to optimize them by collapsing sets of faces [71], by optimizing based on length and angle of integral curves [72], any by binary programming [73]. Finally, manual intervention can be used to establish singular point connectivity where necessary [14,59,74].

1.2. Contributions

In this work, a global reparameterization technique is defined and employed in rebuilding both trimmed and faceted geometries of industrial relevance. Unlike many other global reparameterization methods, however, it does not require the use of mixed-integer optimization, and the resulting parameterization is guaranteed to have a well-defined inverse locally. Specifically, we make the following contributions.

- We define a set of generalized criteria on a triangulation that, if satisfied, yield a quadrilateral layout on the surface (Section 2).
- In Section 3.3, we present a set of partial differential equations that, in combination with Ricci flow, yield a quadrilateral layout-inducing parameterization on a faceted surface.
- We employ the technique in Section 4 to extract trim-free spline surfaces from the US Army's trimmed CAD model of the Unclassified DEVCOM Generic Hull vehicle [35] and from the National Crash Analysis Center's (NCAC's) finite element model of a 1996 Dodge Neon [44]. Extracted spline spaces include ones for which previous methods are known to fail (see [14] and [75, Appendix B]).
- Additionally, in Section 4 we demonstrate, using the isogeometric analysis capabilities in the commercial solver LS-DYNA, that the defined spline surfaces are suitable for use in isogeometric shell analysis.

The first contribution gives a general characterization that, if met, ensures that the computed parameterization on a triangulation defines a quadrilateral layout. The second provides an alternative approach for computing such a parameterization. The third and fourth demonstrate the potential of the proposed technique in creating isogeometric analysis-suitable shells from trimmed and faceted models. Finally, conclusions and future work are discussed in Section 5.

2. Definition of a quadrilateral-inducing parameterization

This section is foundational but necessarily mathematical. It utilizes concepts from differential and algebraic topology and geometry with which many readers may not be familiar. We invite readers unfamiliar with this material to scrutinize figures in this section to attain at least a visual comprehension of the ideas.

Because the NURBS-based B-Rep is the predominant computational representation of CAD geometries, the target object of this work is a non-degenerate set of NURBS splines redefining the original geometry without any trimming. This could be thought of as a coarse, curvilinear quadrilateral mesh, called a quadrilateral layout, defined by a set of splines. This characterization emphasizes that each spline is a curvilinear quadrilateral, but leaves the global objective that the splines must fit together precisely along boundaries unaddressed. Such a local-to-global characterization is not amenable for computation, and so a different representation is necessary.

Additionally, the trimmed spline spaces defining a CAD object also are not amenable for computation without weak coupling. As such, these geometries are converted to a feature-aware unstructured surface triangulation by, for example, triangulating individual parametric domains and mapping these triangulations using the surface mapping, taking care that nodes on surface boundaries align appropriately. Given this triangulation, a global parameterization inducing a quadrilateral layout on the surface is defined by the following criteria of Definition 2.1. Two sample parameterizations satisfying all of these criteria are depicted on a contrived example for an annulus in Fig. 3 and for a bracket of the DEVCOM vehicle in Fig. 4. These criteria may best be understood pictorially, and the reader is invited to study Figs. 5 through 9, in conjunction with Figs. 3 and 4 for best comprehension.

Definition 2.1 (*Quad Layout Immersion*). Let S be an oriented, ¹ triangulated surface with a prescribed set of singular points, P. Take G as a graph along edges of S making S - G a (set of) topological disk(s) such that $P \subset G \cup \partial S$ (hereafter called a **cutting graph**). With this representation, we assume that each edge through which G passes is represented as two edges in S - G, and similarly that vertices of S are split into multiple representations in S - G (see Fig. 5). Then a continuous map $\Psi : S - G \to \mathbb{R}^2$ that generates a quadrilateral layout (called a **quad layout immersion**) satisfies the following criteria.

- Q1 Local injectivity: all but a discrete set of points (specifically, not singularities) have a neighborhood that is locally invertible (see Fig. 6).
- **Q2** For each vertex v of the triangulation on S, take U(v) to be the one-ring neighborhood (a.k.a. the closed star [76]) of v, with T a triangle of U(v). For ease of notation, also write U(v) as the set of triangles in the cut representation S G, where now v may be cut, and is to be understood as the vertex incident to T after cutting. Define $\angle(v, \Psi(T))$ as the inner angle of $\Psi(T)$ incident to vertex $\Psi(v)$. Then the following holds:

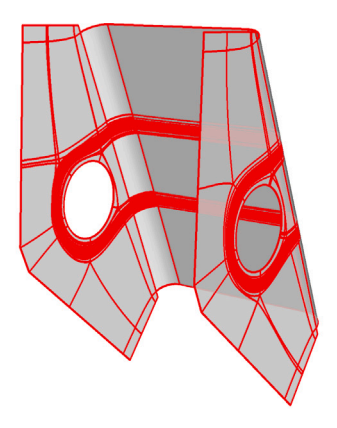
$$\sum_{T\in U(v)} \angle \left(v, \Psi(T)\right) = \begin{cases} 2\pi & \text{if } v \not\in P \text{ and } v \text{ is in the interior of } S \\ \pi & \text{if } v \not\in P \text{ and } v \text{ is on the boundary of } S \\ \frac{k\pi}{2} & \text{for } k \in \mathbb{Z} \text{ if } v \in P \end{cases}$$

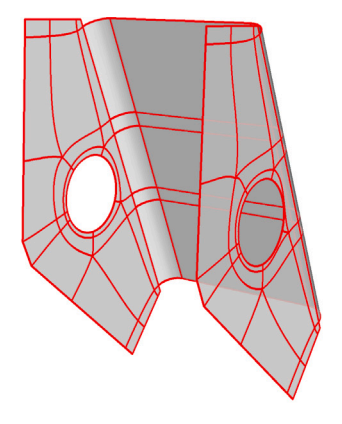
(See Fig. 7 for an example in which k = 5.) Furthermore, a discrete version of the Gauss–Bonnet theorem holds:

(1)

$$\sum_{v \notin \partial S} \left(2\pi - \sum_{T \in U(v)} \angle \left(v, \Psi(T) \right) \right) + \sum_{v \in \partial S} \left(\pi - \sum_{T \in U(v)} \angle \left(v, \Psi(T) \right) \right) = 2\pi \chi(S), \tag{2}$$

 $^{^{1}\,}$ Surfaces of engineering interest are oriented. Non-orientable surfaces are objects like the Möbius band.





(a) Layout without connectivity constraints

(b) Layout with connectivity constraints

Fig. 13. The effects of energy E_5 are demonstrated for a bracket midsurface. Here, two topologically valid layouts are computed—the one on the left without connectivity constraints between singularities and the one on the right with these constraints. The layout without these constraints yields a quadrilateral decomposition with 1898 patches, most of which are slivers and are infeasible for use in design or analysis. The constrained layout, instead, is defined by only 73 patches, and meets needs from both design and analysis perspectives.

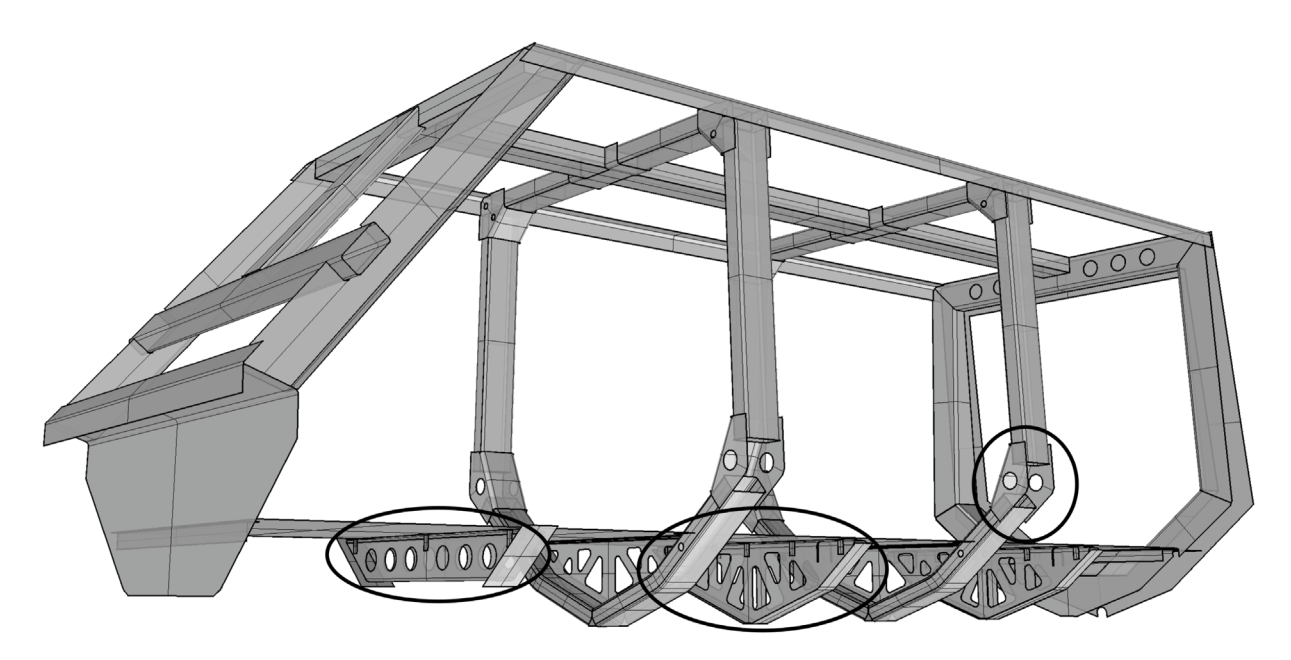


Fig. 14. Three reconstructed parts of the DEVCOM Generic Hull vehicle [35]—two support beams and a bracket of a structural pillar—are shown in the context of the primary support members for the vehicle. All surfaces in this representation are trimmed.

where $\chi(S)$ is the Euler characteristic of the surface.²

- **Q3** Each connected component of $\partial S G$ is mapped by Ψ to a line with constant u or v coordinate (see Fig. 8).
- **Q4** Let each arc of G be written by ω_i , be given an orientation, and be parameterized by arc length. Under S-G, ω_i is represented by ω_{+i} and ω_{-i} on the left and right side of ω_i , respectively, with parameterization consistent with ω_i . Then $\Psi\left(\omega_{-i}(t)\right) = \mathcal{T}\left(\Psi\left(\omega_{+i}(t)\right)\right)$ for $\mathcal{T}: \mathbb{R}^2 \to \mathbb{R}^2$ a translation and rotation by $\frac{k\pi}{2}$, $k \in \mathbb{Z}$ (see Fig. 8).
- Q5 Lines emanating from singularities under the immersion with constant u or v coordinate value, when pulled back to S-G, either
 - 1. Terminate at a (possibly identical) singularity

- 2. Terminate transversely to the boundary
- 3. Are transverse to the cutting graph G

In the final case, the line is continued inductively across the cut using the transformation \mathcal{T} prescribed in Item Q4 (see Fig. 9). All such sets of lines are finite, i.e. they achieve Item (1) or (2) twice.³ The set of these curves emanating from singularities are frequently called **separatrices**.

Furthermore, if these conditions hold, then any curve generated as in Item **Q5** at any point on the surface will be finite (either periodic, part of the separatrices, or terminating transverse to two boundaries). These curves are called **isocontours** or **integral curves**.

These criteria are presented in the smooth setting in [77]. The prescribed set of vertices *P* are called **cone singularities**. If the set of cone

² Recall that for a triangulated surface with V vertices, E edges, and F faces, $\chi(S) = V - E + F$, and is a topological invariant.

 $^{^3}$ In the case that S is an annulus with no singularities or a torus with no singularities, the same holds after artificially calling an arbitrary regular point the surface's only singularity and proceeding as before.

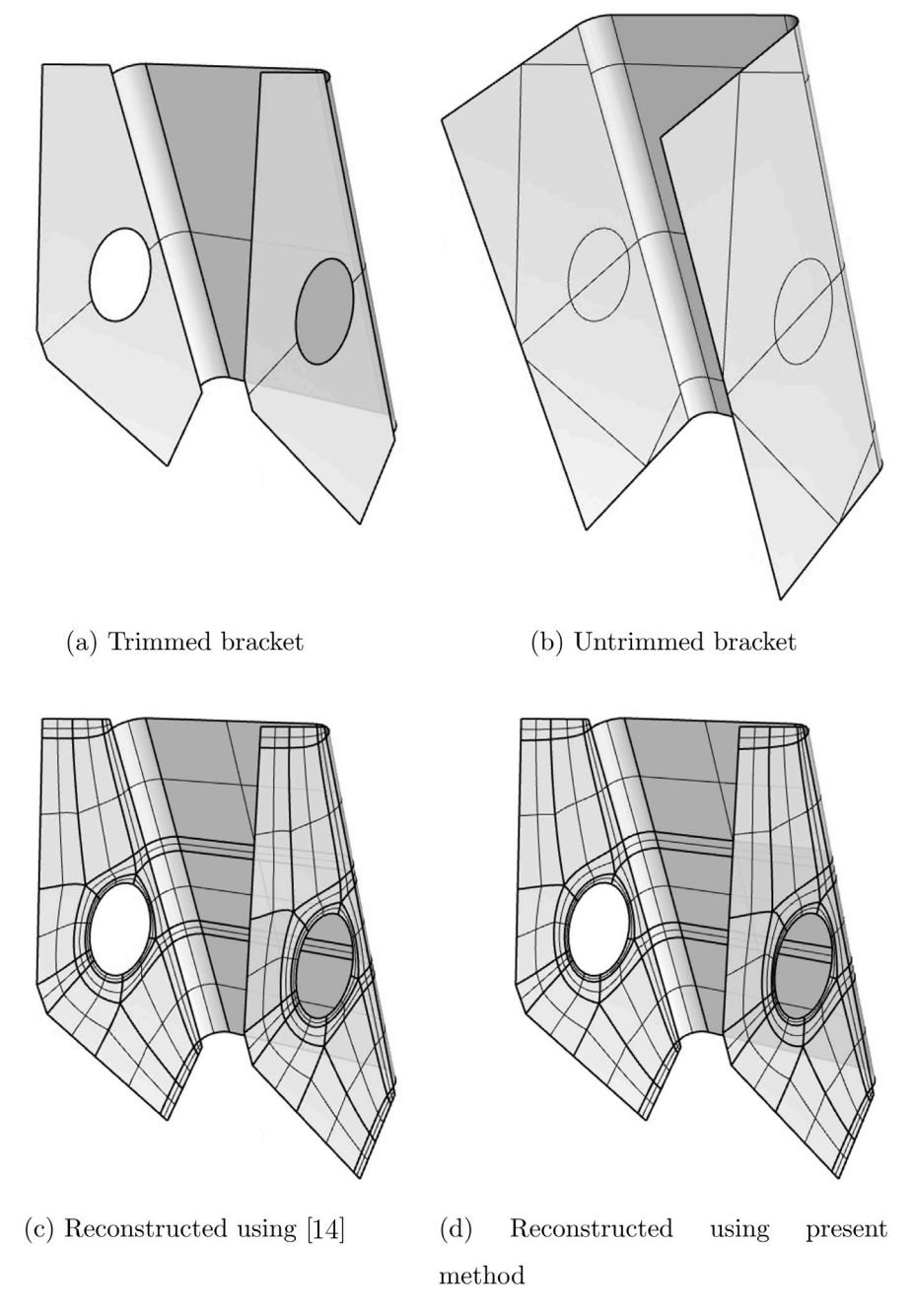


Fig. 15. A bracket of the DEVCOM Generic Hull vehicle is converted into a trim-free watertight spline representation. Below, the reconstruction technique of [14] is compared against that of this method: all splines depicted are Bézier patches. Notice that while singularity locations for both are the same, the integral curves of this approach, being more conformal, are less straight than those of [14], which minimizes a Dirichlet-type energy.

singularities satisfies Eq. (2), it is said that the set is "admissible". Property Q3 is referred to as the boundary-alignment constraint. For frame field-based parameterization methods, Property Q1 is referred to as integrability of a frame field [78]. Properties Q1, Q2, and Q4 together define a so-called "seamless surface parameterization" [79]. Property Q5 is frequently satisfied by obeying integer-grid constraints [48,49, 51,53,68]. Alternative characterizations of a quadrilateral layout as a special Riemannian metric on a surface and as a meromorphic quartic differential are given in [70,80,81], respectively.

In a spline parameterization, the aforementioned cone singularities are referred to as "extraordinary points" or "star points", particularly when located in the interior of the surface. The **valence** of a spline node is defined as the number of spline edges emanating from the node. Extraordinary points correspond to boundary nodes whose valence is not three, or interior nodes with valence not equal to four. Because

extraordinary points are not commonly defined on boundaries and because these cone singularities live on the surface triangulation, we define the **index** of a vertex, v, on the surface triangulation as

$$I(v) = \begin{cases} \frac{2}{\pi} \left(2\pi - \sum_{T \in U(v)} \angle (v, \Psi(T)) \right) & \text{if } v \notin \partial S \\ \frac{2}{\pi} \left(\pi - \sum_{T \in U(v)} \angle (v, \Psi(T)) \right) & \text{if } v \in \partial S. \end{cases}$$
 (3)

Accompanying the index, the following Gauss–Bonnet condition holds, which is equivalent to that in Property **Q2**:

$$\sum_{v \in S} I(v) = 4\chi(S). \tag{4}$$

The index is an integer-valued function defining the discrete contribution of a point to the surface's total curvature. Regular points have index zero, while cone singularities will have non-zero values. A cone

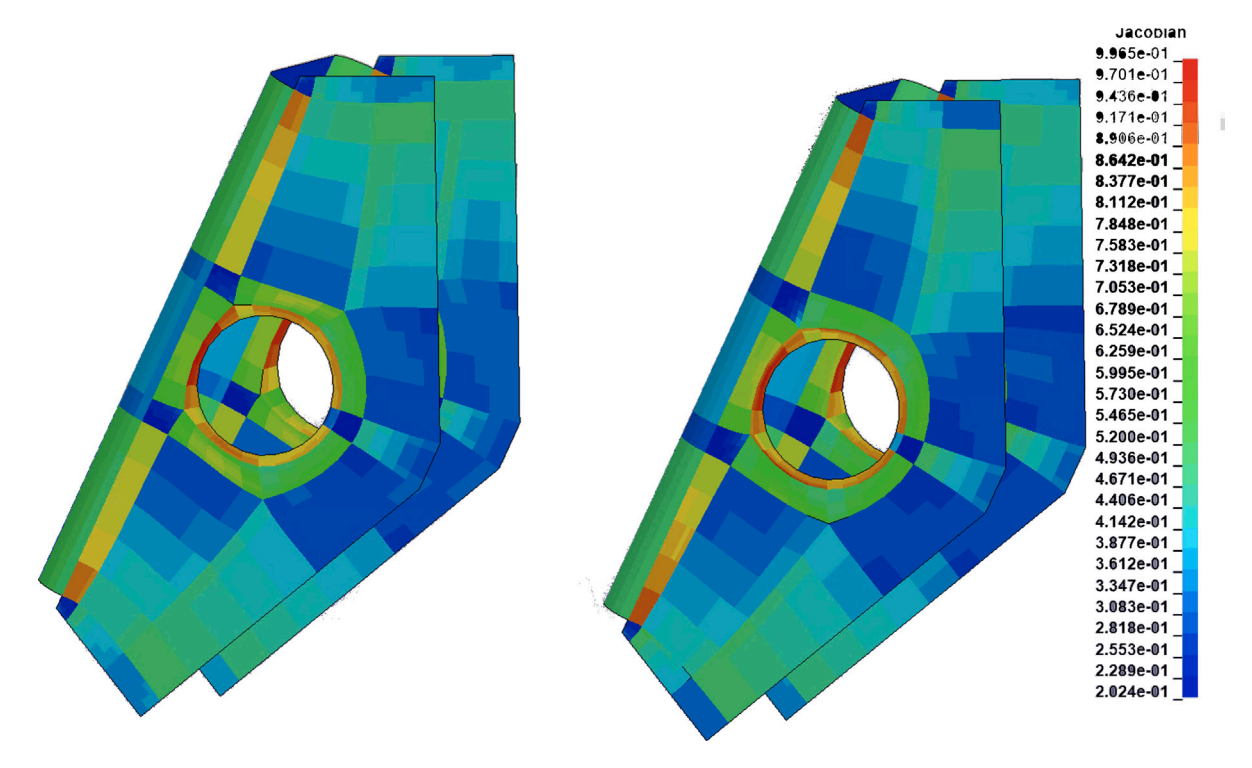


Fig. 16. Jacobians within patches of the DEVCOM bracket rebuilt using the frame field method of [14] (left) and the proposed method of this work (right) are shown. (For interpretation of the references to color in this figure legend, the reader is referred to the web version of this article.)

singularity v corresponds to a point of valence 4 - I(v) if v is in the interior of S, and a point of valence 3 - I(v) if it is on the boundary.

Definition 2.1, though long and a bit arduous, provides a global, computationally-amenable framework for defining a quadrilateral surface parameterization. Given this characterization, the following section defines a set of partial differential equations used to produce such a parameterization.

3. Computation

Given the global recharacterization of a quadrilateral layout as a special type of immersion mapping into the Euclidean plane, as described in Definition 2.1, we proceed to define how to realize this characterization. Fig. 10 walks through this reconstruction process for a contrived yet instructive example of a plate with a hole and a single feature curve, and will be referred to throughout this section.

3.1. Selection of singular points

After having extracted a feature-aware triangulation of the B-Rep (or having subdivided a faceted mesh into a triangulation), a set of singular points must be defined that obey the Gauss–Bonnet condition of Eq. (2) (or equivalently Eq. (4)). For surfaces, this discrete Gauss–Bonnet condition is analogous to the discrete Poincaré–Hopf theorem for frame fields presented in [33,82].

For this work, we employ the frame field method of [14], which combines aspects of [33,34], to automatically place a set of cone singularities. When the prescribed mesh is sufficiently smooth, the results of [33] guarantee that an admissible set of cones is prescribed. However, if the mesh lacks smoothness, has a number of features, or requires prescription of extraordinary points not of valence three or five, manual adjustment may need to be performed. Additionally, the engineer should check to see if the cones are placed in geometrically meaningful locations; if not, the problematic cones should be repositioned for a higher-quality spline reconstruction. For instance, Fig. 11(a) shows cone singularities automatically computed using the

frame field method of [14]: while many singularities are well-placed, some cluster in a way that would benefit from singularity merger, and additional singularities must be introduced because the mesh lacks smoothness necessary to guarantee the Gauss–Bonnet condition of [33]. Instead, these automatically computed singularity positions for a Dodge Neon firewall are manually adjusted to satisfy Gauss–Bonnet, for better positioning, and to combine clustered low-valence singularities into higher-valence ones. All cones of the reference example, Fig. 10, were placed manually. Better placement of these cones in an automatic or semi-automatic manner for featured geometries is a topic for future research.

3.2. Discrete surface Ricci flow

After selection of an admissible set of cone singularities (obeying the Gauss–Bonnet condition of Eq. (2)), a flat metric on the surface with cone singularities is computed using discrete surface Ricci Flow [83–87]. A thorough discussion of discrete surface Ricci flow is presented in [86], with a generalization to less regular meshes given in [87]. Here we briefly review the basic concepts related to this flow.

3.2.1. Ricci Computation

Every surface, S, embedded in \mathbb{R}^3 with a triangulation, \mathfrak{T} , inherits the Riemannian metric of \mathbb{R}^3 . Here, each face T_{ijk} with vertices v_i, v_j, v_k inherits lengths from Euclidean space and angles obeying the typical law of cosines:

$$\ell_{ij}^2 = \ell_{jk}^2 + \ell_{ki}^2 - 2\ell_{jk}\ell_{ki}\cos\left(\angle(v_k, T_{ijk})\right) \tag{5}$$

where ℓ_{ij} is the length of the edge between v_i and v_j , and $\angle(v_k, T_{ijk})$ is the interior angle of triangle T_{ijk} at vertex v_k . Take $\mathfrak V$ as the set of all vertices in the surface triangulation.

Defining the discrete Gaussian curvature at a vertex on the surface to be

$$K_{i} \equiv K(v_{i}) = \begin{cases} 2\pi - \sum_{T \in \mathfrak{T}, v_{i} \in T} \angle(v_{i}, T) & \text{if } v_{i} \notin \partial S \\ \pi - \sum_{T \in \mathfrak{T}, v_{i} \in T} \angle(v_{i}, T) & \text{if } v_{i} \in \partial S, \end{cases}$$
(6)

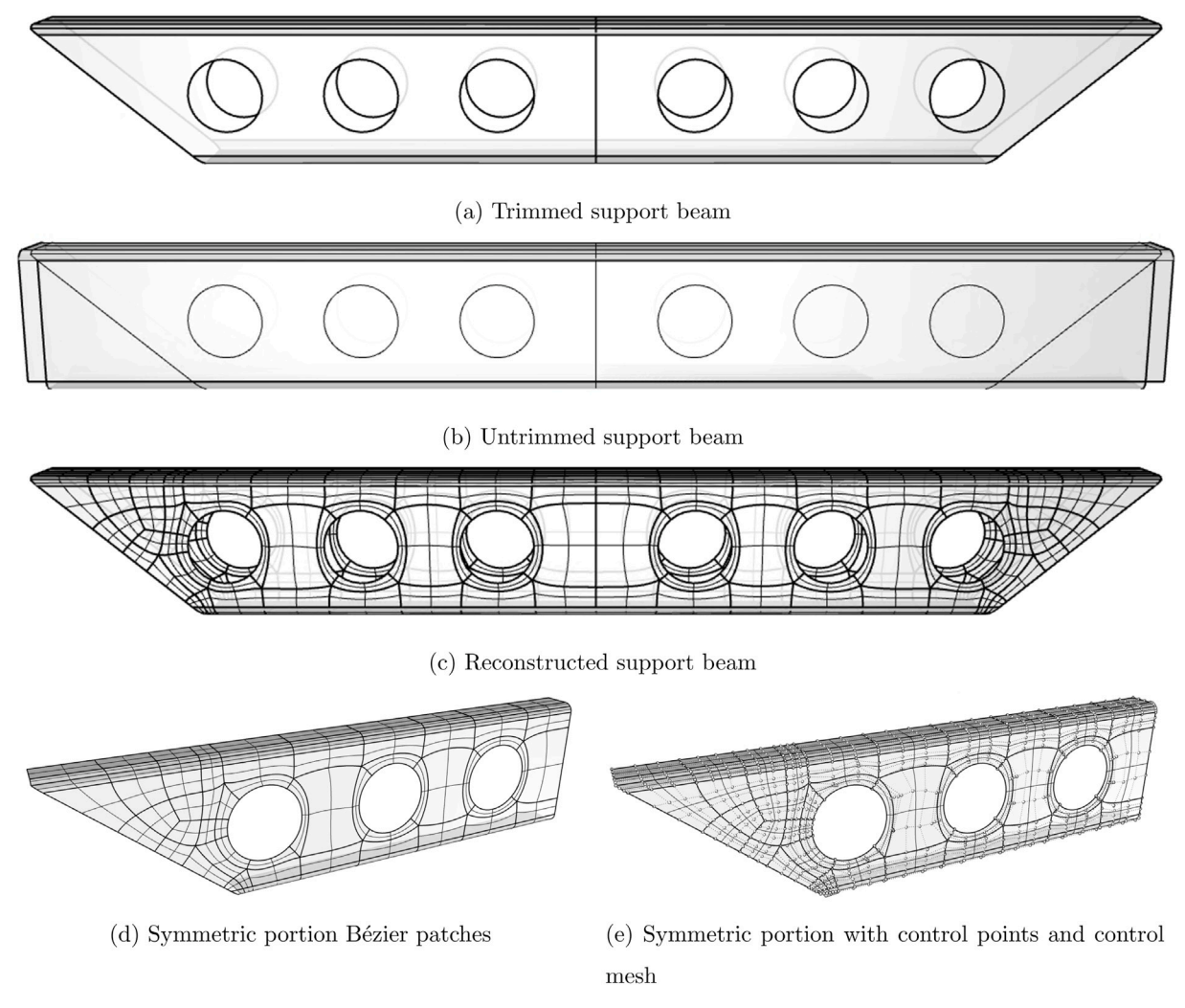


Fig. 17. A structural beam of the DEVCOM Generic Hull vehicle is converted into a trim-free watertight spline representation using bicubic Bézier patches.

then the following discrete Gauss-Bonnet theorem holds [88, p. 252–253]:

$$\sum_{\nu_i \in \mathfrak{V}} K_i = 2\pi \chi(S). \tag{7}$$

From here, a parameter γ_i is selected for each v_i : this represents the length of the radius of a circle about v_i for a discrete circle-packing metric on the surface [83,86,87]. Taking a conformal factor

$$u_i = \log\left(\gamma_i\right) \tag{8}$$

(with potential choices of u_i given in [86,87]), discrete Euclidean surface Ricci flow is governed by the following nonlinear, partial differential equation:

$$\frac{\partial u_i}{\partial t} = \bar{K}_i - K_i,\tag{9}$$

where \vec{K}_i is the input target curvature. Recall that in this instance, \vec{K}_i will be zero for all non-singular points and predefined based on the type of cone singularity for all other points.

Alternatively, discrete surface Ricci flow can be recast as the unique minimizer of the following convex energy,

$$E(u) = \int_0^u \sum_{i=1}^n (\bar{K}_i - K_i), \tag{10}$$

where n is the number of vertices in \mathfrak{V} . Computationally, only a critical point of this energy is needed, meaning that the exact integral never needs to be computed. This can effectively be done using Newton-like methods as in [86,87].

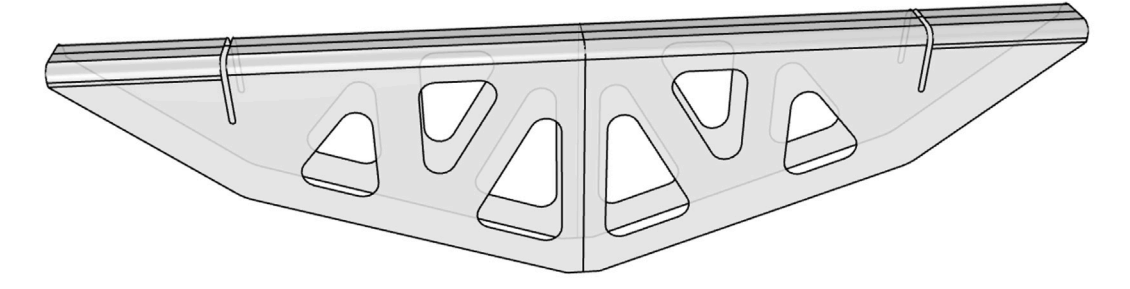
3.2.2. Metric immersion

Upon solving for each u_i by minimizing Eq. (10), the surface has a flat metric with cone singularities. This is converted to an immersion mapping into the two-dimensional Euclidean plane by transforming the computed conformal factors to circle radii (using Eq. (8)), and using a fixed, conformal edge weight $\cos(\phi_{ij})$ in conjunction with the following law of cosines (see Fig. 12):

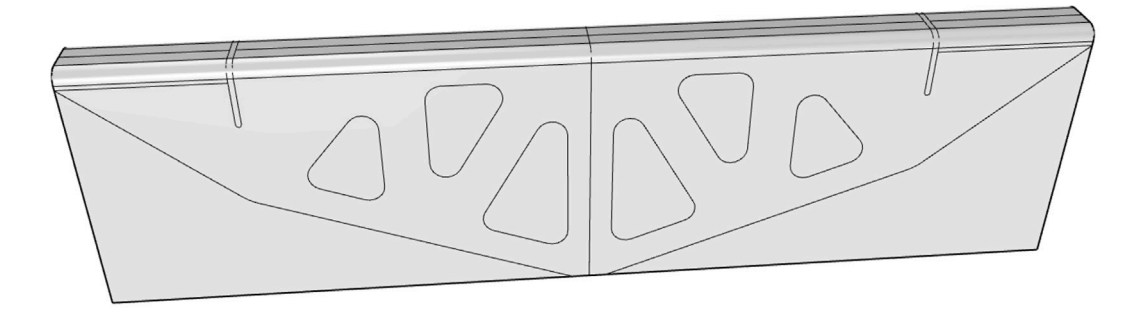
$$\mathcal{E}_{ij}^2 = \gamma_i^2 + \gamma_j^2 + 2\gamma_i \gamma_j \cos(\phi_{ij}). \tag{11}$$

After one surface triangle, T, has been immersed into the plane with arbitrary rotation, neighboring triangles are then mapped into the plane and glued to an edge of T in a similar manner. Proceeding until all surface faces have been visited once will effectively define a map from a cut version of the surface into the Euclidean plane. For the sake of computational simplicity, it is often preferable that these cuts go to, but not through singular points (meaning that a small neighborhood of every singular point is a single connected component under the cutting operation). Recall the set of these cuts, G, is the cutting graph.

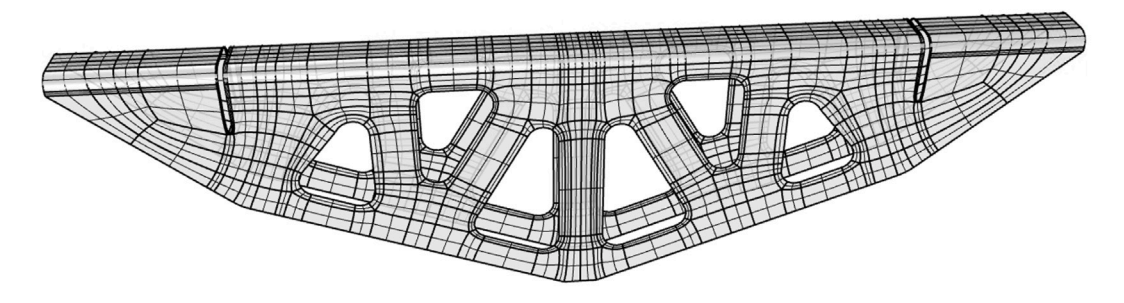
For genus zero surfaces with boundary, the surface can be immersed into the Euclidean plane using this metric to satisfy Properties Q1, Q2, and Q4 of Definition 2.1 [80], leaving only boundary-alignment, feature alignment, and finite-length integral curves to be addressed. More general surfaces will of necessity only satisfy Properties Q1 and Q2. Because we always assume that the surfaces here are open shells (so genus zero with boundaries), we additionally assume that there is an edge in the boundary of S that, under this immersion mapping, has constant u or v coordinate; if not, perform a rotation to make this true.



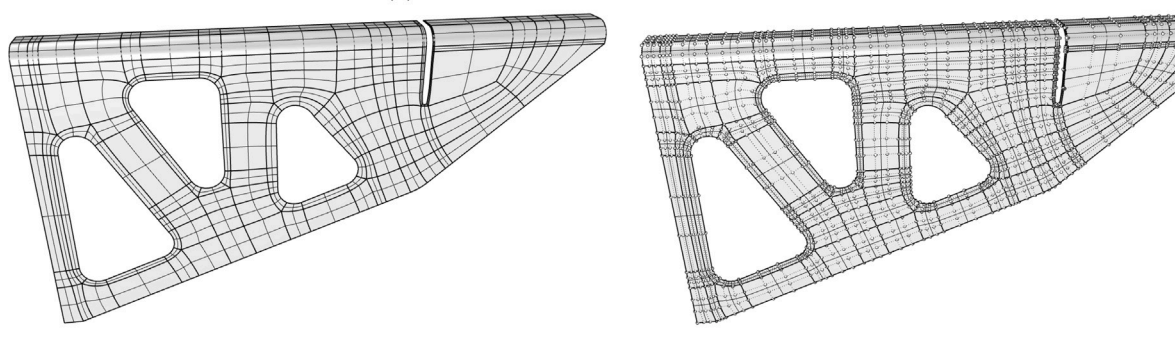
(a) Trimmed rounded support beam



(b) Untrimmed rounded support beam



(c) Reconstructed rounded support beam



(d) Symmetric portion Bézier patches

(e) Symmetric portion with control points and control mesh

Fig. 18. A rounded structural support beam of the DEVCOM Generic Hull vehicle is converted into a trim-free watertight spline representation using bicubic Bézier patches.

Fig. 10(b) depicts the immersion of a cut version of a plate with a hole—Subfigure (a)—into the Euclidean plane based on surface Ricci flow. Here, cuts to cone singularities are shown in red (edges 4, 5, 7, 8, 15 and 16), while cuts to make the surface a topological disk are given by edges in blue (edges 2 and 10). This computed map is locally injective, but does not induce a feature-aligned quadrilateral layout because the

feature curve, curve "a", is not constant in either u or v coordinate. Furthermore, the edge boundaries on the reentrant corners of the L-shaped immersion are not actually constant in u or v, though they are nearly so. This immersion will be transformed into the quadrilateral layout-inducing parameterization of Fig. 10(c) using the following techniques.

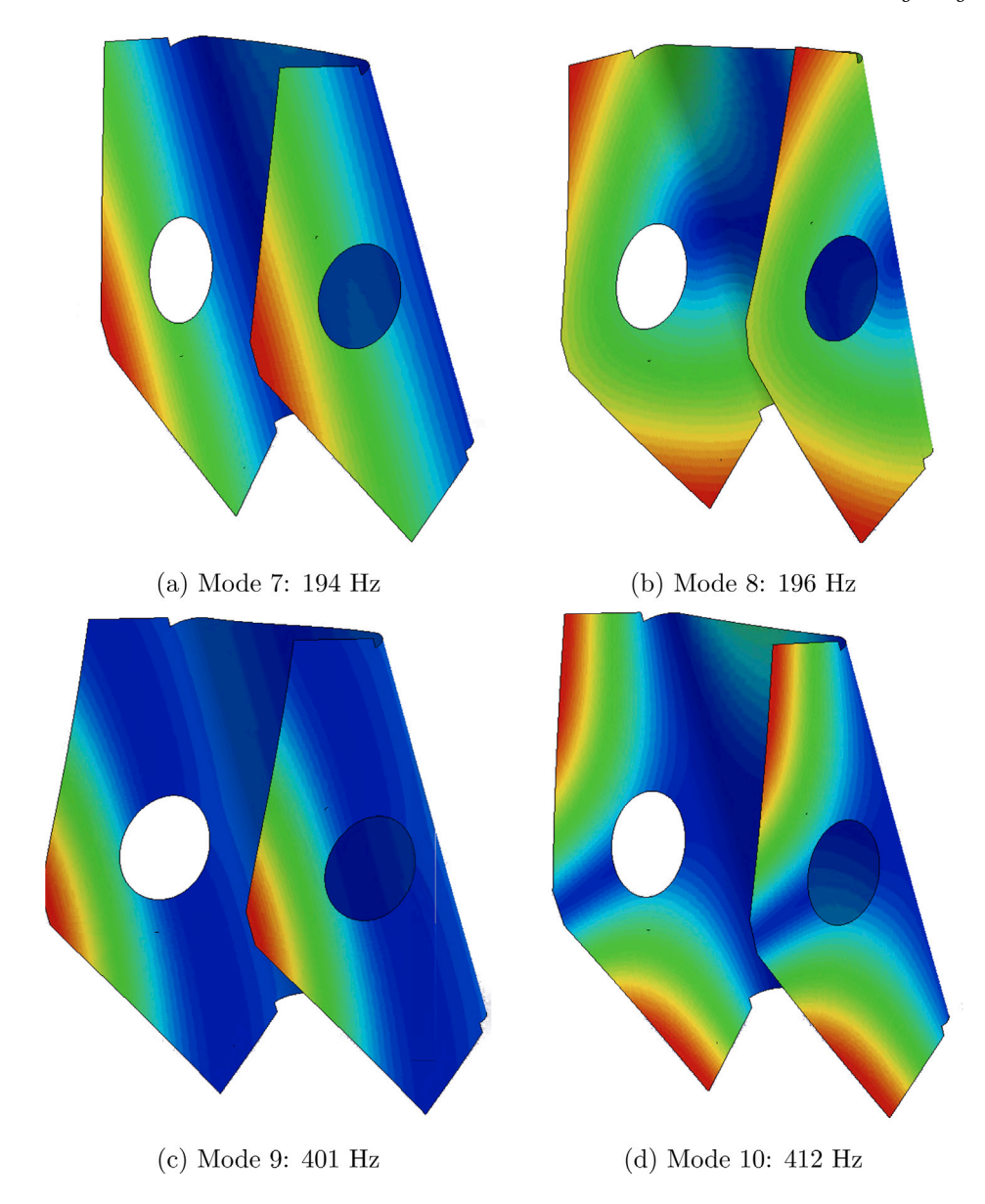


Fig. 19. Isogeometric modal analyses of the reparameterized bracket of Fig. 15(d) with each Bézier patch uniformly subdivided to have 8×8 patches by insertion of knots with single multiplicity. (For interpretation of the references to color in this figure legend, the reader is referred to the web version of this article.)

3.3. Minimization against a layout-inducing energy

Having parameterized the surface by immersing it into the plane, it now remains to transform this parameterization into one that induces a quadrilateral layout, and thus meets all of the requirements of Definition 2.1.

Because all of Definition 2.1 must be enforced, there will accordingly be a variety of constraints on surface subdomains. These subdomains will be written using the following symbols: Γ_u , Γ_v , $\Gamma_u^{\text{feature}}$, $\Gamma_v^{\text{feature}}$, and Γ_{Hol_k} , $k \in \{0,1,2,3\}$. Each of these constrained subdomains is geometric in nature and can easily be visualized: without this appeal to geometry, however, the notation can be heavy. To alleviate this susue, we first present these subdomains on our reference example, Fig. 10, prior to defining the minimization problem and the definition of these symbols. It may be helpful to refer to Fig. 10 throughout this section. In this figure, boundary curves 1,3,9,11, and 13 comprise the set Γ_u , boundary curves 6,12,14, and 17 comprise Γ_v , and the feature curve "a" defines $\Gamma_v^{\text{feature}}$. The edges of 4 and 5 should be related to one another via Γ_{Hol_1} or Γ_{Hol_3} (depending on which side is used as reference). Similarly, edges 7 and 8 should be related to one another

via $\Gamma_{\mathrm{Hol_1}}$ or $\Gamma_{\mathrm{Hol_3}}$, edges 2 and 10 should be related using $\Gamma_{\mathrm{Hol_2}}$, and edges 15 and 16 should be related using $\Gamma_{\mathrm{Hol_2}}$. Both $\Gamma_u^{\mathrm{feature}}$ and $\Gamma_{\mathrm{Hol_0}}$ are empty.

Additionally, note that the Ricci parameterization (Fig. 10(b)) and the quadrilateral-layout inducing parameterization (Fig. 10(c)) both have regions that lie on top of one another, shown with magenta hatching—particularly near the interior cone singularities. Nonetheless, both parameterizations are locally invertible, non-degenerate, and preserve the surface orientation with the mapping. As a result, non-singular locations in the domain have a well-defined inverse mapping with positive Jacobian.

Having established a point of reference for notation, we now proceed defining the minimization problem with its relevant subdomains in the general setting. Let Ω be the domain of the cut surface, S-G, and $\psi_R:\Omega\to\mathbb{R}^2$ be the immersion mapping defined by Ricci flow. Take

$$\mathfrak{F} = \{ \varphi : \Omega \to \mathbb{R}^2, \varphi \in C^0(\Omega), \varphi \text{ locally invertible} \}.$$
 (12)

This defines the set of continuous maps that have a well-defined inverse map. For functions in this family, take $u: \Omega \to \mathbb{R}$ as the parametric u

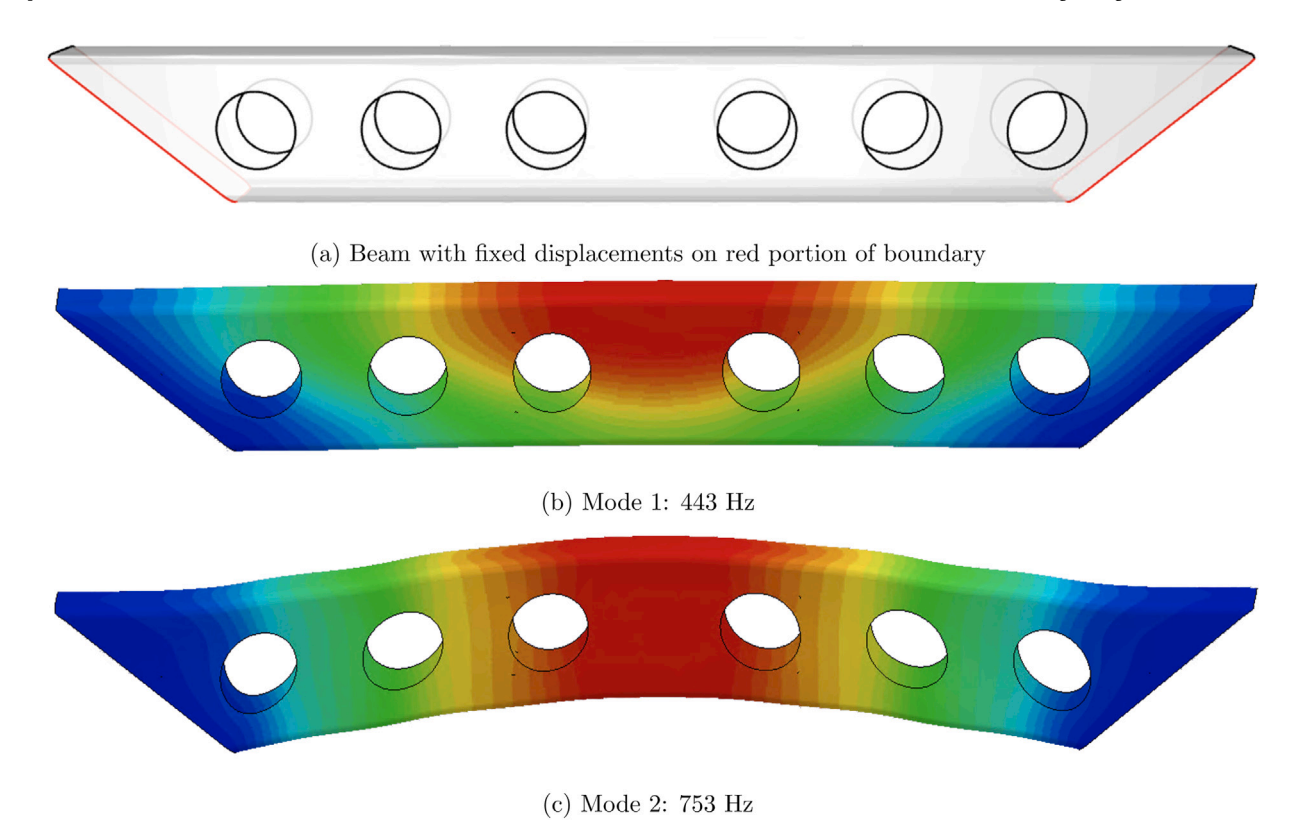


Fig. 20. Isogeometric modal analysis of the reparameterized structural beam of Fig. 17 with pinned supports (zero displacements) on the red portion of the boundary. The Bézier patches of Fig. 17 were uniformly subdivided into 8×8 patches by insertion of knots with single multiplicity. (For interpretation of the references to color in this figure legend, the reader is referred to the web version of this article.)

coordinate of the function, $v:\Omega\to\mathbb{R}$ as the parametric v coordinate. Call a vertex, edge, or face of Ω the child of some parent vertex, edge, or face in S if both the child and parent occupy the same space in \mathbb{R}^3 . Notice that for edges in G, there will be two children edges of G corresponding to a single edge of G, as seen in Fig. 5.

Take e_{ij} as an edge in Ω between vertices v_i and v_j in which $|u(v_i)-u(v_j)| \leq |v(v_i)-v(v_j)|$ and e_{ij} has a parent in ∂S . Define the set of all such edges as Γ_u , and take the all edges in Ω whose parents are also in ∂S but not belonging to Γ_u as Γ_v . Let feature curves of S (and thus of Ω) similarly be classified as members of $\Gamma_u^{\text{feature}}$ based on whether the flux across them is greater in v or in u, respectively.

Similarly, let β be a continuous path in $G \subset S$ with start and end points that are one of the following

- · singular points,
- transverse to a boundary of S, or
- do not have two children in Ω .

Take each interior vertex of the path to have two children in Ω . Thus, each path β will have two continuous children paths in Ω , and each child path will have exactly one child of edges contained in $\beta \subset G$. Define γ as one of these children, ω as the other, and take $\tau(\gamma)$ as the unique translation taking one child vertex of γ to its corresponding sibling in ω , v_{ω} . Define $R_{\hat{k}}, \hat{k} \in \{0,1,2,3\}$ as a rotation by $\frac{\hat{k}\pi}{2}$ radians about v_{ω} . Take k to be number for which the rotation by R_k minimizes the deviation between ω and $R_k(\tau(\gamma))$. Set Γ_{Hol_k} to be the set of all such β paths in which the rotation R_k is used.

Lastly, assume an input set of path connectivity constraints to be enforced between points p,q in the parameterization—typically between singular or feature points that should be connected by an integral curve. These path constraints should be defined in the homotopy class of S-P that they are intended to follow, though the precise path is not important. The paths may be cut by G, and the primary direction of each subcurve under the parameterization mapping may differ across

cuts; these subcurves must be consistently oriented to form a continuous, smooth curve on the branched covering space of the surface [69] defining the quadrilateral layout. Call the set of such constraints Γ_{topo} . Note that each subcurve γ_i of the topologically constrained curve $\gamma_1 \cdot (\dots) \cdot \gamma_\ell$ will be bounded by G, p, or q.

Based on this information, the parameterization sought minimizes the following energy.

Find $\psi \in \mathfrak{F}$ such that

$$\psi = \min_{\varphi \in \mathfrak{F}} \sum_{i=1}^{5} \lambda_j E_j \tag{13}$$

with

$$E_1(\varphi) = \int_{\Omega} \|J\|_F^2 + \|J^{-1}\|_F^2 d\Omega$$
 (14)

$$E_2(\varphi) = \int_{\Gamma} \left(\frac{\partial u}{\partial s}\right)^2 d\Gamma + \int_{\Gamma} \left(\frac{\partial v}{\partial s}\right)^2 d\Gamma \tag{15}$$

$$E_3(\varphi) = \int_{\Gamma_u^{\text{feature}}} \left(\frac{\partial u}{\partial s}\right)^2 d\Gamma + \int_{\Gamma_v^{\text{feature}}} \left(\frac{\partial v}{\partial s}\right)^2 d\Gamma$$
 (16)

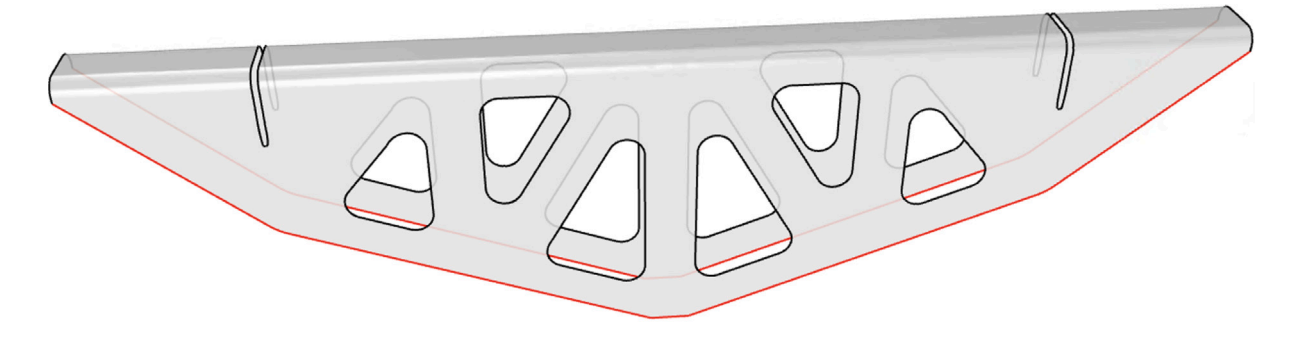
$$E_{4}(\varphi) = \sum_{k=0}^{3} \sum_{(\beta \in \Gamma_{\text{Hol}_{k}})} \int_{\beta} \left(\frac{\partial \varphi_{+}}{\partial s} - R_{k}^{-1} \left(\frac{\partial \varphi_{-}}{\partial s} \right) \right) \cdot \left(\frac{\partial \varphi_{+}}{\partial s} - R_{k}^{-1} \left(\frac{\partial \varphi_{-}}{\partial s} \right) \right) \partial \Gamma$$

$$(17)$$

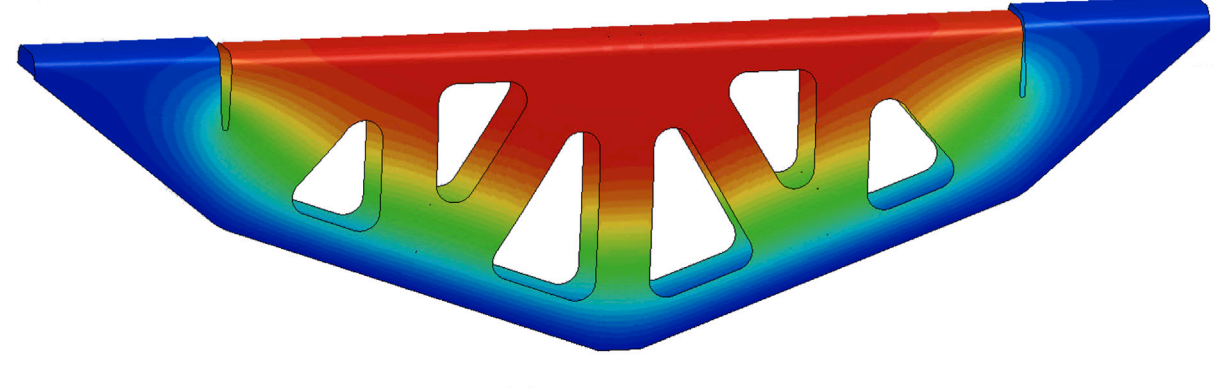
 $E_5(\varphi) = \sum_{\gamma_1 \cdot (\dots) \cdot \gamma_{\ell} \in \Gamma_{\text{topo}}} \left(\sum_{j=1}^{\ell} \int_{\gamma_j} \frac{\partial \varphi_{j_k}}{ds} d\Gamma \right)^2$ (18)

$$= \sum_{\gamma_{1}\cdot(\dots)\cdot\gamma_{\ell}\in\Gamma_{\text{topo}}} \left(\sum_{j=1}^{\ell} \varphi_{j_{k}}\left(\gamma_{j}(1)\right) - \varphi_{j_{k}}\left(\gamma_{j}(0)\right)\right)^{2}. \tag{19}$$

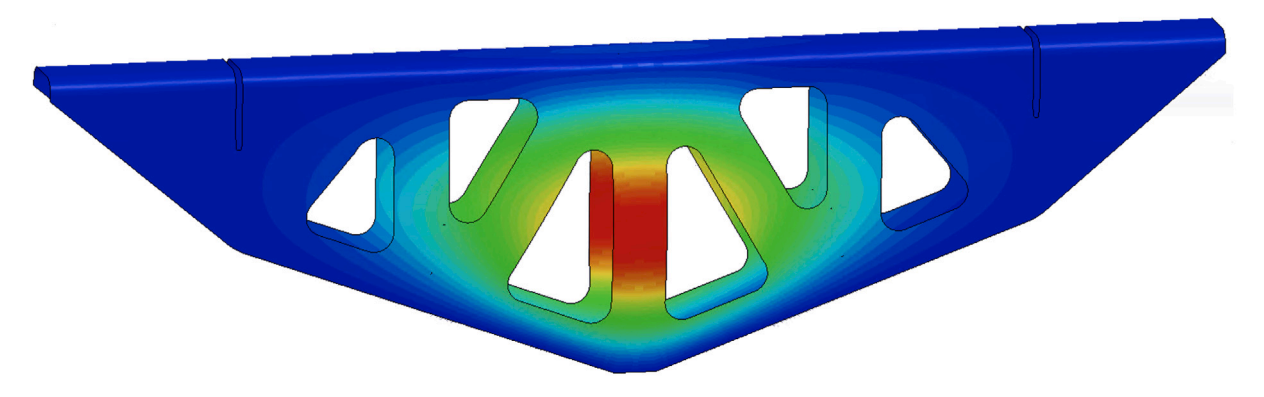
Here, J is the Jacobian transformation from Ω to $\mathbb R$ (local to each triangle), with $\|J\|_F$ representing the Frobenius norm, and φ_{j_k} is the constrained direction and orientation (k=0 is +u, k=1 is +v, k=2 is -u and k=3 is -v) for the subcurve γ_j . The first energy aims



(a) Beam with fixed displacements on red portion of boundary



(b) Mode 1: 132 Hz



(c) Mode 2: 323 Hz

Fig. 21. Isogeometric modal analysis of the reparameterized structural beam of Fig. 18 with pinned supports (zero displacements) on the red portion of the boundary. The Bézier patches of Fig. 18 were uniformly subdivided into 8×8 patches by insertion of knots with single multiplicity. (For interpretation of the references to color in this figure legend, the reader is referred to the web version of this article.)

for a smooth deformation $(\|J\|_F^2$ term) while also ensuring that local injectivity is preserved $(\|J^{-1}\|_F^2$ term), and is called the symmetric Dirichlet energy [89]. It preserves Property **Q1** of Definition 2.1. The next energy ensures boundary-alignment constraints, and helps satisfy Property **Q3**. Energy E_3 gives control over feature alignment, and ensures that features of the triangulation (preserved from the B-Rep) are preserved. Next, energy E_4 enforces Properties **Q2** and **Q4**. Finally, energy E_5 can be used to satisfy Property **Q5**.

Remark 3.1. For the purposes of generating a quadrilateral layout on a midsurface, energy E_5 may not be absolutely necessary in that a quadrilateral layout on the surface may be found without enforcing any connectivity constraints. However, such unconstrained layouts will seldom meet downstream needs for design and analysis due to quadrilaterals of arbitrarily poor aspect ratios, as demonstrated in Fig. 13.

Energy E_5 precludes such poor layout configurations on open surfaces. For closed surfaces, these constraints are necessary to ensure that a valid quadrilateral partitioning can be generated.

The above energy is non-linear with penalty terms, and can be minimized using Newton-like iteration. Note that the initial parameterization guess, ψ_R , will not exactly satisfy many of the necessary constraints, so constraints transforming it into a quadrilateral layout must be enforced weakly. Because a Nitsche formulation will not generally yield the exact satisfaction of these constraints (which is necessary for the parameterization to yield a layout, as in Definition 2.1), we instead opt for iteratively solving using a penalty method. Here, as $\lambda_j \to \infty$ for $j=2,\dots,5$ the parameterization converges to enforcing exact constraint satisfaction. For all operations, $\lambda_1=1$ is selected to preserve local injectivity, while the other penalty terms are gradually increased. This minimization problem can be solved efficiently using

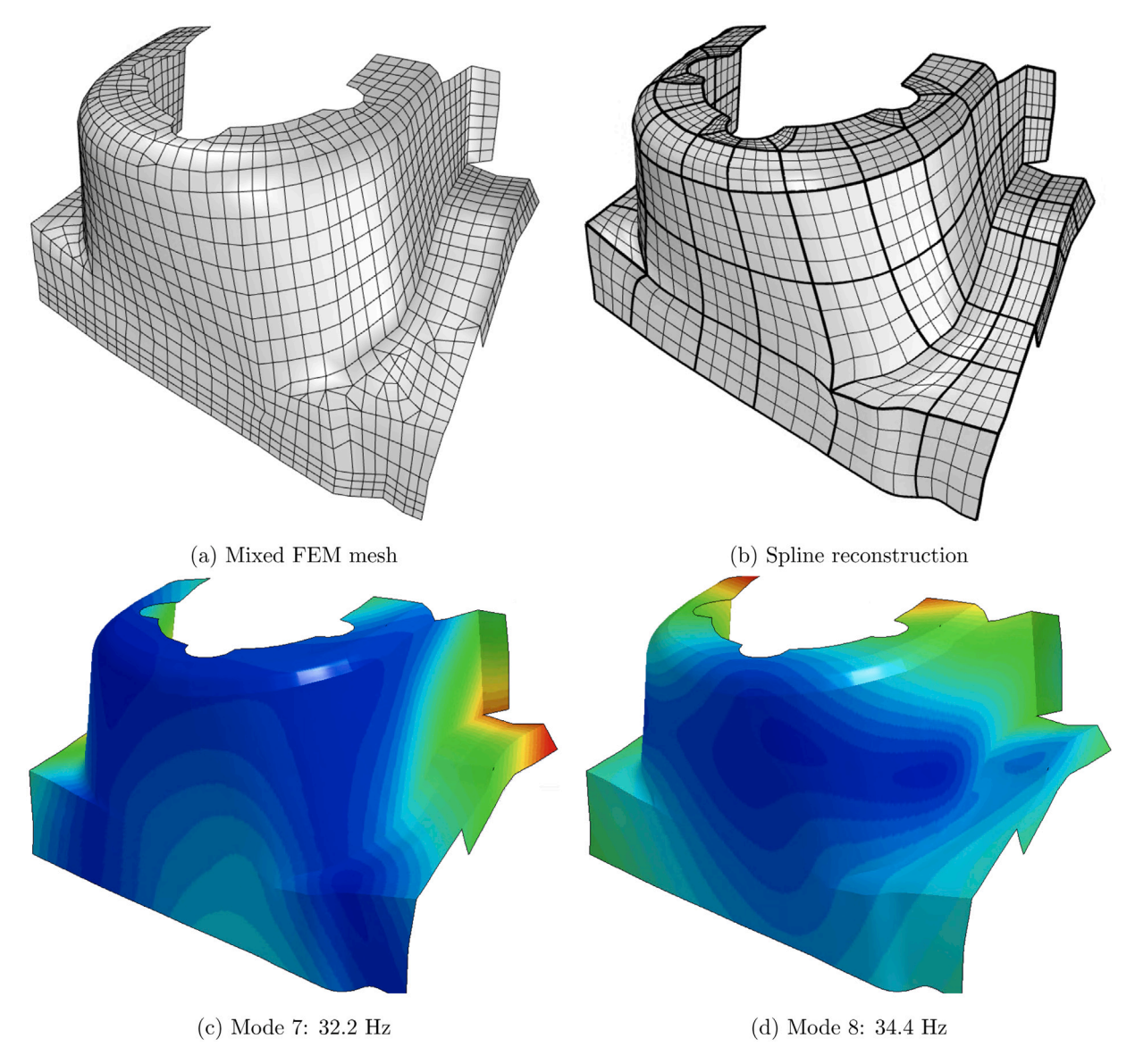


Fig. 22. The front right shock house from a finite element mesh of a 1996 Dodge Neon [44] is rebuilt as a set of bicubic NURBS patches, each with 7×7 control points (i.e. 4×4 Bézier patches), with at least C^2 continuity on the interior of each patch and C^0 continuity between patches. After uniform refinement to 8×8 Bézier patches for each patch, modal analysis is performed on the model with free boundaries. (For interpretation of the references to color in this figure legend, the reader is referred to the web version of this article.)

techniques such as [90–92]. It is often valuable to switch J between referencing the Euclidean geometry of the surface and the Ricci metric of the surface to extract the solutions of subsequent minimizations with increased lambda values from local minima.

4. Results

We demonstrate the efficacy of the proposed framework by reconstructing both trimmed and faceted models of industrial vehicles into trim-free spline representations suitable for isogeometric analysis. Here, integral lines emanating from singular points, from feature vertices, and along boundaries are extracted from the surface triangulation's parameterization, yielding a feature-aware quadrilateral partitioning of the surface. From here, cubic spline curves are fit using a least squares approximation of the integral lines. Lastly, surfaces are extracted using Coons patch interpolation. As such, all B-Reps have C^0 continuity between adjacent patches, and at least C^2 continuity in their interiors.

4.1. DEVCOM Generic Hull

The US Army's DEVCOM Generic Hull vehicle was created in an initiative to involve academia and industry in the research of undervehicle blast phenomena without the challenges posed by operating on classified material [35]. The entire vehicle is comprised of an outer hull with various structural beams and pillars composing the structural frame. The midsurfaces of a structural bracket and two beams were extracted from the frame for reconstruction, shown in reference to the rest of the vehicle's primary structural members in Fig. 14.

The bracket, which has been reconstructed in [14] using a global frame field-based approach, is shown in Fig. 15. Here, it is shown in its trimmed form, its untrimmed form, and its reconstructed form using the present method. Additionally, its form after reconstruction using the method of [14] is presented for reference. While both the layout computed using Ricci flow with metric optimization and the layout of [14] have singular points in the same locations, the frame field layout produces integral curves that are more geodesic on the original geometry, while the proposed method is more biased to the geodesic

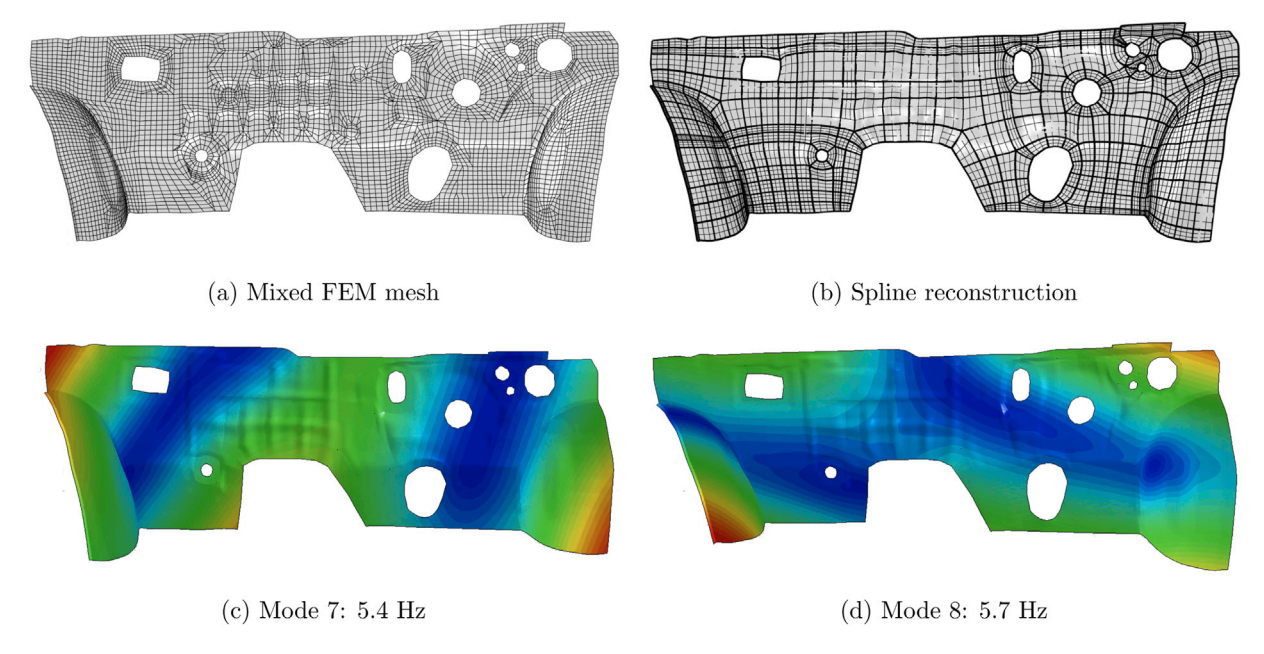


Fig. 23. The cabin firewall from a finite element mesh of a 1996 Dodge Neon [44] is rebuilt as a set of bicubic NURBS patches, each with 6×6 control points (i.e. 3×3 Bézier patches), with at least C^2 continuity on the interior of each patch and C^0 continuity between patches. After uniform refinement to 12×12 Bézier patches for each patch, modal analysis is performed on the model with free boundaries. (For interpretation of the references to color in this figure legend, the reader is referred to the web version of this article.)

curvature of the nearby boundary. As seen in Fig. 16, both methods yield splines whose Jacobians are comparable.

Both rebuilt beams are also depicted with their trimmed and untrimmed representations (see Figs. 17 and 18). However, the frame field method of [14] failed to produce a valid parameterization for these models, so the layouts produced from this work are not compared against an alternative global reparameterization technique.

For analysis, each bicubic Bézier patch was uniformly refined into a bicubic NURBS patch with 8×8 Bézier patches each using single-multiplicity knot insertion. Implicit modal analysis was performed using LS-DYNA. All parts analyzed are shells of thickness 6.350 mm, and are made of ASTM A36 Steel, which has the following properties.

- Modulus of Elasticity (E): 2.07 · 10⁵ MPa
- Mass Density (ρ): $7.8 \cdot 10^3$ kg/m³
- Poisson's Ratio (v): 0.33

Analyses use the Reissner–Mindlin shell formulation. The bracket is taken with no boundary conditions (Fig. 19), so has six rigid body displacement modes. Both of the other analyses assume boundary constraints as depicted in their accompanying figures (Figs. 20 and 21).

4.2. 1996 Dodge Neon

George Washington University's National Crash Analysis Center (NCAC) has performed a variety of finite element crash simulations for evaluation of safety of a number of commercial vehicles. One such model is the 1996 Dodge Neon [44], which was tested for frontal crash loading.

Though hundreds of parts comprise the actual vehicle, this work focuses on the evaluation of four: the vehicle firewall, the cabin's rear deck speaker support, the front-right shock house, and the outer-right shell member of the vehicle's chassis. These parts were selected due to their geometric and topological complexity. For each of these models, the original faceted model and the reconstructed watertight B-Rep are displayed side-by-side in Subfigures (a) and (b), respectively, of Figs. 22, 23, 24, and 25.

When starting from a finite element mesh, geometric errors that are a by-product of feature removal, geometry clean-up, and other approximations typically made to facilitate finite element mesh generation are obviously inherited by the spline model. The sharp crease in Fig. 22 and the sharp reentrant corners in the holes of Fig. 25 are manifestations of this. Nevertheless, the spline models eliminate all triangles in FEM meshes, which are a liability in local nonlinear failure analysis, and thus are a significant improvement. However, many of these geometric errors can be fixed by smoothly mapping the spline model to the original CAD geometry. An L^2 -best fitting would seem a simple and efficient procedure for this purpose. This is a topic for future research

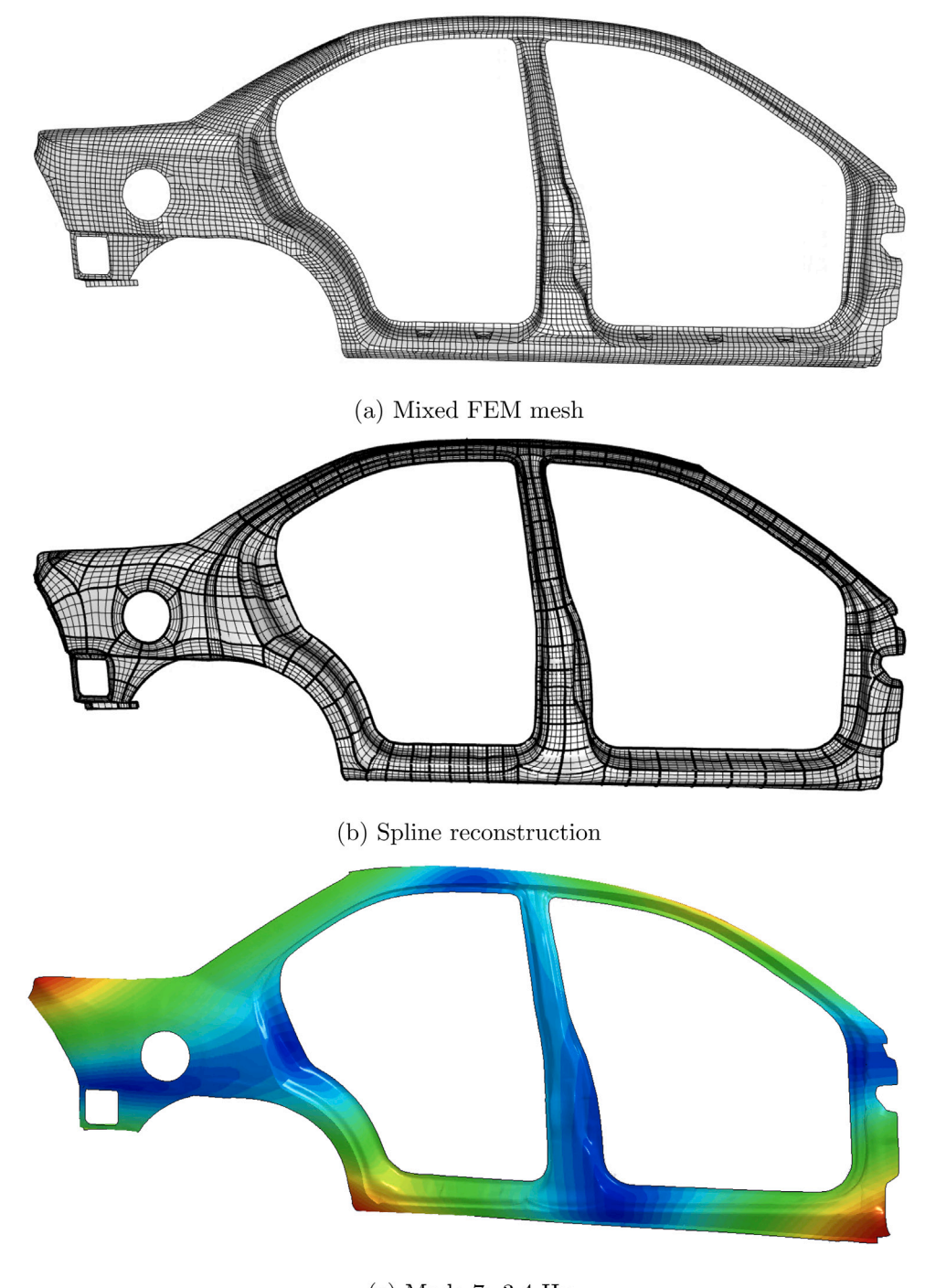
Isogeometric modal analyses are performed for refinements of each of the above-listed models. All analyses use the Reissner–Mindlin shell formulation. Material data for the NCAC finite element model, which was also used in these isogeometric analyses, was determined from coupon testing [44]: the analyzed parts are all steel. All analyzed models have following mass density, modulus of elasticity, and Poisson's ratio:

- Modulus of Elasticity (E): 2.1 · 10⁵ MPa
- Mass Density (ρ): 7.89 · 10³ kg/m³
- Poisson's Ratio (v): 0.30

Thicknesses of shells are 0.735, 0.829, 0.96, and 0.907 mm, respectively. Representative modes for the spline models are shown in the latter subfigures of Figs. 22, 23, 24, and 25.

5. Conclusions

In this work, we presented a new framework to rebuild trimmed and faceted open midsurface geometries into isogeometric analysis-suitable spline spaces. First, we defined a generalized set of criteria for a surface triangulation that, if satisfied, generate a quadrilateral layout. Based on this theory, we combined the tools of discrete surface Ricci flow [86,87] with a constrained minimization against an inversion-precluding energy [89–92] with layout-inducing penalty constraints. The methodology assures that the computed parameterizations are locally injective, a necessary criterion frequently not satisfied by many current quadrilateral parameterization techniques [14,48,49,53,68]. The defined framework was used to rebuild topologically and



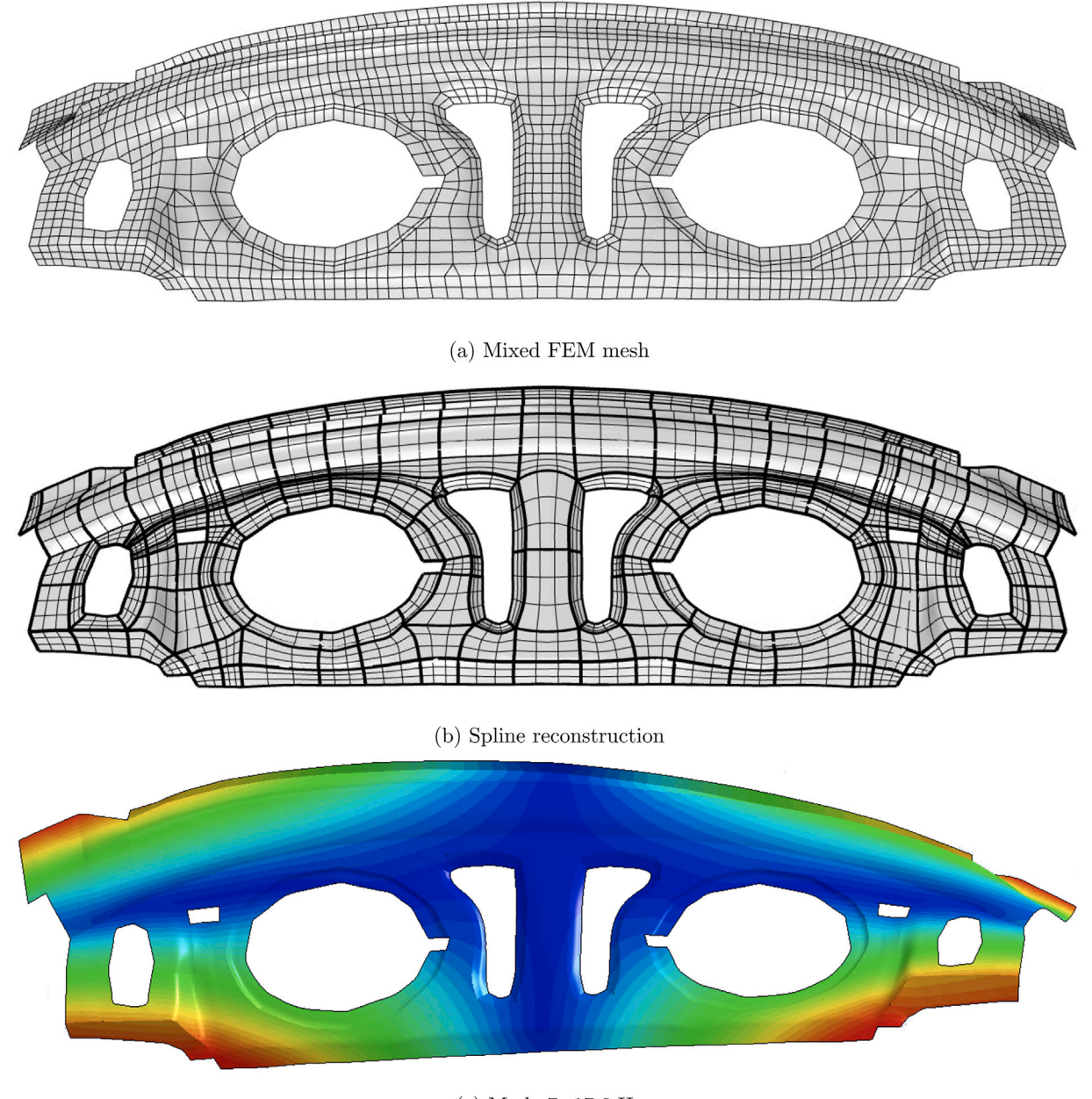
(c) Mode 7: 3.4 Hz

Fig. 24. The right outer shell of the cabin chassis from a finite element mesh of a 1996 Dodge Neon [44] is rebuilt as a set of bicubic NURBS patches, each with 7×7 control points (i.e. 4×4 Bézier patches), with at least C^2 continuity on the interior of each patch and C^0 continuity between patches. After uniform refinement to 8×8 Bézier patches for each patch, modal analysis is performed on the model with free boundaries. (For interpretation of the references to color in this figure legend, the reader is referred to the web version of this article.)

geometrically complicated members of both the US Army's DEVCOM Generic Hull vehicle [35] and the National Crash Analysis Center's 1996 Dodge Neon finite element model [44], including models for which current state-of-the-art techniques fail [75, Appendix B]. We show the viability of each of the rebuilt models by using them for isogeometric modal analyses using the commercial solver LS-DYNA.

While the proposed framework offers a feature-aware technique to generate spline surfaces suitable for isogeometric analysis, additional work remains. First, the proposed methodology focuses on reconstruction of open surfaces. While there is no theoretical reason that

the technique cannot extend to closed surfaces other than potential holonomy issues for unusual and pathological singularity configurations [79,81], the methodology has not yet been explored on these surfaces. Closed surfaces pose an additional challenge, as well, because they will not typically satisfy Property Q5 of Definition 2.1, as will most open surfaces. A forthcoming work formalizing theory defined in [93] demonstrates that connectivity constraints automatically or semi-automatically defined between singularities can easily fit into the proposed framework. As such, we are optimistic that the proposed



(c) Mode 7: 17.6 Hz

Fig. 25. The frame supporting the rear speakers of the cabin from a finite element mesh of a 1996 Dodge Neon [44] is rebuilt as a set of bicubic NURBS patches, each with 6×6 control points (i.e. 3×3 Bézier patches), with at least C^2 continuity on the interior of each patch and C^0 continuity between patches. After uniform refinement to 12×12 Bézier patches for each patch, modal analysis is performed on the model with free boundaries. (For interpretation of the references to color in this figure legend, the reader is referred to the web version of this article.)

technique can also easily incorporate the automatic connectivity constraints defined in [53,70], particularly because both of these methods operate on an initial seamless surface parameterization, which kind of parameterization is exactly produced herein.

Next, the parameterization framework needs alternative ways to select singularities. The current framework relies on a Dirichlet-type energy with guarantees for valid singularity positions only if the input geometry is sufficiently smooth [33]: these smoothness conditions may not hold on highly-featured structural and mechanical surfaces. Furthermore, automatic placement of singularities is limited to valence three and five singularities [33], though many geometries of interest may benefit from higher-valence cones. Future research will explore alternative ways to robustly compute cone singularities for featured surfaces, including evaluating existing techniques proposed in [49,70, 94–96].

Finally, additional research should focus on more advanced spline fitting techniques. The current technique employs linear interpolation between integral curves defining the boundary of a patch in the quadrilateral layout. For more nonlinear parameterizations or geometries with significant curvature in their domains, this technique will be insufficient to capture these nonlinear features and would require additional layout subdivision at the expense of more degrees of freedom and reduced continuity. Instead, manifold splines such as unstructured T-splines [97–99] or U-splines [100] may be necessary. Additional research will also need to focus on how to fit splines produced on the triangulation back to the original trimmed CAD domain. Because geometries used herein are predominantly flat, reconstruction from the triangulation to the original geometry was fairly straightforward. An ultimate objective is minimizing the need for user intervention in the process.

CRediT authorship contribution statement

Kendrick M. Shepherd: Conceptualization, Methodology, Software, Validation, Formal analysis, Investigation, Data Curation, Writing – original draft, Writing – review & editing, Visualization. **Xianfeng David Gu:** Resources, Writing – review & editing, Supervision. **Thomas J.R. Hughes:** Conceptualization, Resources, Writing – review & editing, Supervision, Project Administration, Funding acquisition.

Declaration of competing interest

The authors declare that they have no known competing financial interests or personal relationships that could have appeared to influence the work reported in this paper.

Acknowledgments

The authors would like to thank Attila Nagy and the team at LS-DYNA for their assistance performing isogeometric modal analyses.

Thomas J. R. Hughes and Kendrick Shepherd were partially supported by United States Department of Defense Navy Contract N6833518C0014 through a subcontract with Coreform, LLC, which is gratefully acknowledged.

References

- Luo X, Shephard M, Remacle J-F. Influence of geometric approximation on the accuracy of higher order methods. Technical report, Troy, NY: Scientific Computation Research Center, Rensselaer Polytechnic Institute; 2001.
- [2] Boggs PT, Althsuler A, Larzelere AR, Walsh EJ, Clay RL, Hardwick MF. DART system analysis. Report, Sandia National Laboratories; 2005, http://dx.doi.org/ 10.2172/876325
- [3] Farouki RT. Closing the gap between CAD model and downstream application. SIAM News 1999;32(5):1–3, URL https://archive.siam.org/news/news.php?id=
- [4] Brunnermeier SB, Martin SA. Interoperability cost analysis of the US automotive supply chain. Supply Chain Manag. 2002;7(2):71–82. http://dx.doi.org/10. 1108/13598540210425821.
- [5] Babuška I, Suri M. Locking effects in the finite element approximation of elasticity problem. Numer Math 1992;62:439–63. http://dx.doi.org/10.1007/ BE01306238
- [6] Hughes TJR, Reali A, Sangalli G. Duality and unified analysis of discrete approximations in structural dynamics and wave propagation: Comparison of p-method finite elements with k-method NURBS. Comput Methods Appl Mech Engrg 2008;197(49–50):4104–24.
- [7] Belytschko T, Liu WK, Moran B, Elkhodary K. Nonlinear finite elements for continua and structures. second ed.. New York: John Wiley & Sons, Inc.; 2014.
- [8] Hughes TJR, Cottrell JA, Bazilevs Y. Isogeometric analysis: CAD, finite elements, NURBS, exact geometry and mesh refinement. Comput Methods Appl Mech Engrg 2005;194(39–41):4135–95. http://dx.doi.org/10.1016/j.cma.2004. 10.008.
- [9] Kiendl J, Bletzinger K-U, Linhard J, Wuchner R. Isogeometric shell analysis with Kirchhoff-Love elements. Comput Methods Appl Mech Engrg 2009;198(49–52):3902–14. http://dx.doi.org/10.1016/j.cma.2009.08.013.
- [10] Nguyen-Thanh N, Valizadeh N, Nguyen MN, Nguyen-Xuan H, Zhuang X, Areias P, et al. An extended isogeometric thin shell analysis based on kirchhoff-love theory. Comput Methods Appl Mech Engrg 2015;284:265–91. http://dx.doi.org/10.1016/j.cma.2014.08.025.
- [11] Evans JA, Bazilevs Y, Babuška I, Hughes TJR. n-Widths, sup-infs, and optimality ratios for the k-version of the isogeometic finite element method. Comput Methods Appl Mech Engrg 2009;198(21–26):1726–41. http://dx.doi.org/10. 1016/j.cma.2009.01.021.
- [12] Sande E, Manni C, Speleers H. Sharp error estimates for spline approximation: Explicit constants, n-widths, and eigenfunction convergence. Math Models Methods Appl Sci 2019;29(6):1175–205. http://dx.doi.org/10.1142/S0218202519500192.
- [13] Sande E, Manni C, Speleers H. Explicit error estimates for spline approximation of arbitrary smoothness in isogeometric analysis. Numer Math 2020;144:889–929. http://dx.doi.org/10.1007/s00211-019-01097-9.
- [14] Hiemstra RR, Shepherd KM, Johnson MJ, Quan L, Hughes TJR. Towards untrimmed NURBS: CAD embedded reparameterization of trimmed B-rep geometry using frame-field guided global parameterization. Comput Methods Appl Mech Engrg 2020;369:113227. http://dx.doi.org/10.1016/j.cma.2020.113227.

- [15] Puzyrev V, Deng Q, Calo V. Spectral approximation properties of isogeometric analysis with variable continuity. Comput Methods Appl Mech Engrg 2018;334:22–39. http://dx.doi.org/10.1016/j.cma.2018.01.042.
- [16] Beirão da Veiga L, Hughes TJR, Kiendl J, Lovadina C, Niiranen J, Reali A, et al. A locking-free model for Reissner–Mindlin plates: Analysis and isogeometric implementation via NURBS and triangular NURPS. Math Models Methods Appl Sci 2015;25(8):1519–51. http://dx.doi.org/10.1142/S0218202515500402.
- [17] Oesterle B, Ramm E, Bischoff M. A shear deformable, rotation-free isogeometric shell formulation. Comput Methods Appl Mech Engrg 2016;307:235–55. http: //dx.doi.org/10.1016/j.cma.2016.04.015.
- [18] Zou Z, Hughes TJR, Scott MA, Sauer RJ, Savithac EJ. Galerkin formulations of isogeometric shell analysis: Alleviating locking with greville quadratures and higher-order elements. Comput Methods Appl Mech Engrg 2021;380. http: //dx.doi.org/10.1016/j.cma.2021.113757.
- [19] Zou Z, Scott MA, Miao D, Bischoff M, Oesterle B, Dornisch W. An isogeometric Reissner-Mindlin shell element based on Bézier dual basis functions: Overcoming locking and improved coarse mesh accuracy. Comput Methods Appl Mech Engrg 2020;370. http://dx.doi.org/10.1016/j.cma.2020.113283.
- [20] Farin G. Curves and surfaces for CAGD: A practical guide. fifth ed.. San Francisco, CA: Morgan Kaufmann Publishers; 2002, http://dx.doi.org/10.1016/ B978-1-55860-737-8.X5000-5.
- [21] Brunnett G. Geometric design with trimmed surfaces. In: Hagen H, Farin G, Noltemeier H, editors. Geometric modelling. Computing supplement, vol. 10, Springer; 1989, p. 101–15. http://dx.doi.org/10.1007/978-3-7091-7584-2_7.
- [22] Marussig B, Hughes TJR. A review of trimming in isogeometric analysis: Challenges, data exchange and simulation aspects. Arch Comput Methods Eng 2017;25:1–69. http://dx.doi.org/10.1007/s11831-017-9220-9.
- [23] Kim H-J, Seo Y-D, Youn S-K. Isogeometric analysis for trimmed CAD surfaces. Comput Methods Appl Mech Engrg 2009;198(37–40):2982–95. http://dx.doi. org/10.1016/j.cma.2009.05.004.
- [24] Nagy AP, Benson DJ. On the numerical integration of trimmed isogeometric elements. Comput Methods Appl Mech Engrg 2015;284:165–85. http://dx.doi. org/10.1016/j.cma.2014.08.002.
- [25] Rank E, Ruess M, Kollmannsberger S, Schillinger D, Düster A. Geometric modeling, isogeometric analysis and the finite cell method. Comput Methods Appl Mech Engrg 2012;249–252:104–15. http://dx.doi.org/10.1016/j.cma.2012.05.022.
- [26] Guo Y, Heller J, Hughes TJR, Ruess M, Schillinger D. Variationally consistent isogeometric analysis of trimmed thin shells at finite deformations, based on the STEP exchange format. Comput Methods Appl Mech Engrg 2018;336:39–79. http://dx.doi.org/10.1016/j.cma.2018.02.027.
- [27] Ruess M, Schillinger D, Bazilevs Y, Varduhn V, Rank E. Weakly enforced essential boundary conditions for NURBS-embedded and trimmed NURBS geometries on the basis of the finite cell method. Internat J Numer Methods Engrg 2013;95(10):811–46. http://dx.doi.org/10.1002/nme.4522.
- [28] Ruess M, Schillinger D, Özcan AI, Rank E. Weak coupling for isogeometric analysis of non-matching and trimmed multi-patch geometries. Comput Methods Appl Mech Engrg 2014;269:46–71. http://dx.doi.org/10.1016/j.cma.2013.10.
- [29] Schmidt R, Wüchner R, Bletzinger K-U. Isogeometric analysis of trimmed NURBS geometries. Comput Methods Appl Mech Engrg 2012;241–244:93–111. http://dx.doi.org/10.1016/j.cma.2012.05.021.
- [30] Katz S, Sederberg TW. Genus of the intersection curve of two rational surface patches. Comput Aided Geom Design 1988;5(3):253–8. http://dx.doi.org/10. 1016/0167-8396(88)90006-4.
- [31] Sederberg TW, Anderson DC, Goldman RN. Implicit representation of parametric curves and surfaces. Comput Vis Graph Image Process 1984;28(1):72–84. http: //dx.doi.org/10.1016/0734-189X(84)90140-3.
- [32] Sederberg TW, Finnigan GT, Li X, Lin H, Ipson H. Watertight trimmed NURBS. In: ACM SIGGRAPH 2008 papers. SIGGRAPH '08, ACM; 2008, p. 79:1–8. http://dx.doi.org/10.1145/1399504.1360678.
- [33] Knöppel F, Crane K, Pinkall U, Schröder P. Globally optimal direction fields. ACM Trans Graph 2013;32(4):59:1–59:10. http://dx.doi.org/10.1145/2461912. 2462005
- [34] Panozzo D, Puppo E, Tarini M, Sorkine-Hornung O. Frame fields: Anisotropic and non-orthogonal cross fields. ACM Trans Graph 2014;33(4):134:1–134:11. http://dx.doi.org/10.1145/2601097.2601179.
- [35] Dooge D, Dwarampudi R, Schaffner G, Miller A, Thyagarajan R, Madanmohan V, et al. Evolution of occupant survivability simulation framework using FEM-SPH coupling. In: 2011 NDIA Ground Vehicle Systems Engineering and Technology Symposium (GVSETS), Dearborn, MI, Aug 9–11, 2011, DTIC Report #ADA547566, TARDEC Registration #22044.
- [36] Breitenberger M. CAD-integrated design and analysis of shell structures. (Ph.D. thesis), Technical University of Munich, Germany; 2016, URL http://mediatum.ub.tum.de/?id=1311417.
- [37] de Prenter F, Verhoosel CV, van Brummelen EH. Preconditioning immersed isogeometric finite element methods with application to flow problems. Comput Methods Appl Mech Engrg 2019;348:604–31. http://dx.doi.org/10.1016/j.cma. 2019.01.030.

- [38] de Prenter F, Verhoosel CV, van Zwieten GJ, van Brummelen EH. Condition number analysis and preconditioning of the finite cell method. Comput Methods Appl Mech Engrg 2017;316:297–327. http://dx.doi.org/10.1016/j.cma.2016.07. 006
- [39] Marussig B, Hiemstra R, Hughes TJR. Improved conditioning of isogeometric analysis matrices for trimmed geometries. Comput Methods Appl Mech Engrg 2018;334:79–110. http://dx.doi.org/10.1016/j.cma.2018.01.052.
- [40] Marussig B, Zechner J, Beer G, Fries T-P. Stable isogeometric analysis of trimmed geometries. Comput Methods Appl Mech Engrg 2017;316:497–521. http://dx.doi.org/10.1016/j.cma.2016.07.040.
- [41] Breitenberger M, Apostolatos A, Philipp B, Wüchner R, Bletzinger KU. Analysis in computer aided design: Nonlinear isogeometric B-rep analysis of shell structures. Comput Methods Appl Mech Engrg 2015;284:401–57. http://dx.doi. org/10.1016/j.cma.2014.09.033.
- [42] Guo Y, Do H, Ruess M. Isogeometric stability analysis of thin shells: from simple geometries to engineering models. Int J Numer Methods Eng 2019;118(8):433–58. http://dx.doi.org/10.1002/nme.6020.
- [43] Leidinger LF, Breitenberger M, Bauer AM, Hartmann S, Wüchner R, Bletzinger K-U, et al. Explicit dynamic isogeometric B-Rep analysis of penalty-coupled trimmed NURBS shells. Comput Methods Appl Mech Engrg 2019;351:891–927. http://dx.doi.org/10.1016/j.cma.2019.04.016.
- [44] George Washington University. Finite element model of dodge neon. Technical report, George Washington University, Virginia Campus; 2006.
- [45] Randrianarivony M. Geometric processing of CAD data and meshes as input of integral equation solvers. (Ph.D. thesis), Computer Science Faculty Technische Universität Chemnitzn; 2006.
- [46] Randrianarivony M. On global continuity of coons mappings in patching CAD surfaces. Comput Aided Des 2009;41(11):782–91. http://dx.doi.org/10.1016/j. cad.2009.04.012.
- [47] Urick B, Marussig B, Cohen E, Crawford RH, Hughes TJR, Riesenfeld RF. Watertight boolean operations: A framework for creating CAD-compatible gap-free solid models. Comput Aided Design 2019;115:147–60. http://dx.doi.org/10.1016/j.cad.2019.05.034.
- [48] Bommes D, Campen M, Ebke H-C, Alliez P, Kobbelt L. Integer-grid maps for reliable quad meshing. ACM Trans Graph 2013;32(4). http://dx.doi.org/10. 1145/2461912.2462014.
- [49] Bommes D, Zimmer H, Kobbelt L. Mixed-integer quadrangulation. In: ACM SIGGRAPH 2009 papers. SIGGRAPH '09, ACM; 2009, p. 77:1–77:10. http://dx.doi.org/10.1145/1576246.1531383.
- [50] Campen M, Bommes D, Kobbelt L. Dual loops meshing: Quality quad layouts on manifolds. ACM Trans Graph 2012;31(4):110:1–110:11. http://dx.doi.org/ 10.1145/2185520.2185606.
- [51] Campen M, Bommes D, Kobbelt L. Quantized global parameterization. ACM Trans Graph 2015;34(6):192. http://dx.doi.org/10.1145/2816795.2818140.
- [52] Dong S, Bremer P-T, Garland M, Pascucci V, Hart J. Spectral surface quadrangulation. ACM Trans Graph 2006;25(3):1057–66. http://dx.doi.org/10.1145/ 1141911.1141993.
- [53] Lyon M, Campen M, Kobbelt L. Quad layouts via constrained T-mesh quantization. Comput Graph Forum 2021;40(2).
- [54] Benzley SE, Perry E, Merkley K, Clark B, Sjaardema G. A comparison of all hexagonal and all tetrahedral finite element meshes for elastic and elasticplastic analysis. In: Proc. 4th international meshing roundtable. Albuquerque, NM: Sandia National Laboratories; 1995, p. 179–92.
- [55] Shewchuck JR. Triangle: Engineering a 2D mesh generator and delaunay triangulator. In: Lin MC, Manocha D, editors. Applied computational geometry towards geometric engineering. WACG 1996. Lecture notes in computer science, vol. 1148, Springer, Berlin, Heidelberg; 1996, p. 203–22. http://dx.doi.org/10. 1007/BFb0014497.
- [56] Shewchuk JR. Delaunay refinement mesh generation. (Ph.D. thesis), Carnegie Mellon University; 1997.
- [57] Shewchuk JR. General-dimensional constrained delaunay and constrained regular triangulations, I: Combinatorial properties. Discrete Comput Geom 2008;39:580–637. http://dx.doi.org/10.1007/s00454-008-9060-3.
- [58] Hu K, Zhang YJ. Centroidal voroni tessellation based polycube construction for adaptive all-hexahedral mesh generation. Comput Methods Appl Mech Engrg 2016;305:405–21. http://dx.doi.org/10.1016/j.cma.2016.03.021.
- [59] Tong Y, Alliez P, Cohen-Steiner D, Desbrun M. Designing quadrangulations with discrete harmonic forms. In: Proceedings of the fourth eurographics symposium on geometry processing. SGP '06, Eurographics Association; 2006, p. 201–10. http://dx.doi.org/10.2312/SGP/SGP06/201-210.
- [60] Marinov M, Amagliani M, Charrot P. Boundary conforming mesh to T-NURCC surface conversion. Comput Graph 2019;82:94–105. http://dx.doi.org/10.1016/ i.cag.2019.05.012.
- [61] Al Akhras H, Elguedj T, Gravouil A, Rochette M. Towards an automatic isogeometric analysis suitable trivariate models generation—Application to geometric parametric analysis. Comput Methods Appl Mech Engrg 2017;316:623–45. http://dx.doi.org/10.1016/j.cma.2016.09.030.
- [62] Maquart T, Wenfeng Y, Elguedj T, Gravouil A, Rochette M. 3D volumetric isotopological meshing for finite element and isogeometric based reduced order modeling. Comput Methods Appl Mech Engrg 2020;362:112809. http://dx.doi. org/10.1016/j.cma.2019.112809.

- [63] Gu X, Yau S-T. Global conformal surface parameterization. In: Kobbelt L, Schröeder P, Hoppe H, editors. Eurographics symposium on geometry processing. The Eurographics Association; 2003, p. 127–37. http://dx.doi.org/10.2312/ SGP/SGP03/127-137.
- [64] Lei N, Zheng X, Jiang J, Lin Y-Y, Gu DX. Quadrilateral and hexahedral mesh generation based on surface foliation theory. Comput Methods Appl Mech Engrg 2017;316:758–81. http://dx.doi.org/10.1016/j.cma.2016.09.044.
- [65] Lei N, Zheng X, Luo Z, Gu DX. Quadrilateral and hexahedral mesh generation based on surface foliation theory II. Comput Methods Appl Mech Engrg 2017;321:406–26. http://dx.doi.org/10.1016/j.cma.2017.04.012.
- [66] Ray N, Vallet B, Alonso L, Levy B. Geometry-aware direction field processing. ACM Trans Graph 2009;29(1):1:1–1:11. http://dx.doi.org/10.1145/1640443. 1640444
- [67] Shen J, Kosinka J, Sabin M, Dodgson NA. Converting a CAD model into a non-uniform subdivision surface. Comput Aided Geom Design 2016;48:17–35. http://dx.doi.org/10.1016/j.cagd.2016.07.003.
- [68] Ebke H-C, Bommes D, Campen M, Kobbelt L. QEX: Robust quad mesh extraction. ACM Trans Graph 2013;32(6):168:1–168:10. http://dx.doi.org/10.1145/2508363,2508372.
- [69] Kälberer F, Nieser M, Polthier K. QuadCover surface parameterization using branched coverings. Comput Graph Forum 2007;26(3):375–84. http://dx.doi. org/10.1111/j.1467-8659.2007.01060.x.
- [70] Zheng X, Zhu Y, Chen W, Lei N, Luo Z, Gu X. Quadrilateral mesh generation III: Optimizing singularity configuration based on Abel–Jacobi theory. Comput Methods Appl Mech Engrg 2021;387. http://dx.doi.org/10.1016/j.cma.2021. 114146.
- [71] Viertel R, Osting B, Staten M. Coarse quad layouts through robust simplification of cross field separatrix partitions. 2019, arXiv preprint arXiv:1905.09097, arXiv:1905.09097.
- [72] Tarini M, Puppo E, Panozzo D, Pietroni N, Cignoni P. Simple quad domains for field aligned mesh parameterization. ACM Trans Graph 2011;30(6):142. http://dx.doi.org/10.1145/2024156.2024176.
- [73] Razafindrazaka FH, Polthier K. Optimal base complexes for quadrilateral meshes. Comput Aided Geom Design 2017;52–53(C):63–74. http://dx.doi.org/ 10.1016/j.cagd.2017.02.012.
- [74] Campen M, Kobbelt L. Quad layout embedding via aligned parameterization. Comput Graph Forum 2014;33(8):69–81. http://dx.doi.org/10.1111/cgf.12401.
- [75] Hiemstra RR. Enabling higher order isogeometric analysis for applications in structural mechanics. (Ph.D. thesis), Austin, TX: The University of Texas at Austin; 2019, http://dx.doi.org/10.26153/tsw/5857.
- [76] Hudson JFP. Piecewise linear topology. New York, NY: W.A. Benjamin, Inc.;
- [77] Shepherd KM, Hiemstra RR, Hughes TJR. The quad layout immersion: A mathematically equivalent representation of a surface quadrilateral layout. 2020, arXiv preprint arXiv:2012.09368, arXiv:2012.09368.
- [78] Diamanti O, Vaxman A, Panozzo D, Sorkine-Hornung O. Integrable PolyVector fields. ACM Trans Graph 2015;34(4):38:1–38:12. http://dx.doi.org/10.1145/ 2766906.
- [79] Campen M, Shen H, Zhou J, Zorin D. Seamless parametrization with arbitrary cones for arbitrary genus. ACM Trans Graph 2019;39(1). http://dx.doi.org/10. 1145/3360511.
- [80] Chen W, Zheng X, Ke J, Lei N, Luo Z, Gu X. Quadrilateral mesh generation I: Metric based method. Comput Methods Appl Mech Engrg 2019;356:652–68. http://dx.doi.org/10.1016/j.cma.2019.07.023.
- [81] Lei N, Zheng X, Luo Z, Luo F, Gu X. Quadrilateral mesh generation II: Meromorphic quartic differentials and Abel–Jacobi condition. Comput Methods Appl Mech Engrg 2020;366. http://dx.doi.org/10.1016/j.cma.2020.112980.
- [82] Ray N, Vallet B, Li WC, Lévy B. N-symmetry direction field design. ACM Trans Graph 2008;1–13. http://dx.doi.org/10.1145/1356682.1356683.
- [83] Chow B, Luo F. Combinatorial Ricci flows on surfaces. J Differential Geom 2003;63(1):97–129. http://dx.doi.org/10.4310/jdg/1080835659.
- [84] Gu X, Guo R, Luo F, Sun J, Wu T. A discrete uniformization theorem for polyhedral surfaces II. J Differential Geom 2018;109(3):431–66. http://dx.doi. org/10.4310/jdg/1531188190.
- [85] Gu XD, Lou F, Sun J, Wu T. A discrete uniformization theorem for polyhedral surfaces. J Differential Geom 2018;109(2):223–56. http://dx.doi.org/10.4310/ idg/1527040872.
- [86] Jin M, Kim J, Luo F, Gu X. Discrete surface Ricci flow. IEEE Trans Vis Comput Graph 2008;14(5):1030–43. http://dx.doi.org/10.1109/TVCG.2008.57.
- [87] Yang Y-L, Guo R, Luo F, Hu S-M, Gu X. Generalized discrete Ricci flow. Comput Graph Forum 2009;28(7):2005–14. http://dx.doi.org/10.1111/j.1467-8659.2009.01579.x.
- [88] Gu XD, Yau S-T. Computational conformal geometry. In: Yau S-T, Liu K, Ji L, editors. Advanced lectures in mathematics, Vol. 3. Somerville, MA, U.S.A.: International Press; 2008.
- [89] Smith J, Schaefer S. Bijective parameterization with free boundaries. ACM Trans Graph 2015;34(4):70:1–9. http://dx.doi.org/10.1145/2766947.
- [90] Liu L, Ye C, Ni R, Fu X-M. Progressive parameterizations. ACM Trans Graph 2018;37(4):41. http://dx.doi.org/10.1145/3197517.3201331.

- [91] Rabinovich M, Poranne R, Panozzo D, Sorkine-Hornung O. Scalable locally injective mappings. ACM Trans Graph 2017;36:16. http://dx.doi.org/10.1145/ 2983621
- [92] Shtengel A, Poranne R, Sorkine-Hornung O, Kovalsky SZ, Lipman Y. Geometric optimization via composite majorization. ACM Trans Graph 2017;36(4):38:1–38:11. http://dx.doi.org/10.1145/3072959.3073618.
- [93] Shepherd KM. Isogeometric analysis-suitable geometry: Rebuilding CAD surface geometries via quadrilateral layouts. (Ph.D. thesis), The University of Texas at Austin; 2021, http://dx.doi.org/10.26153/tsw/13885.
- [94] Diamanti O, Vaxman A, Panozzo D, Sorkine-Hornung O. Designing N-PolyVector fields with complex polynomials. Comput Graph Forum 2014;33(5):1–11. http://dx.doi.org/10.1111/cgf.12426.
- [95] Jakob W, Tarini M, Panozzo D, Sorkine-Hornung O. Instant field-aligned meshes. ACM Trans Graph 2015;34(6):189. http://dx.doi.org/10.1145/2816795.2818078.
- [96] Viertel R, Osting B. An approach to quad meshing based on harmonic cross-valued maps and the Ginzburg-Landau theory. SIAM J Sci Comput 2019;41(1):A452-79. http://dx.doi.org/10.1137/17M1142703.
- [97] Casquero H, Wei X, Toshniwal D, Li A, Hughes TJR, Kiendl J, et al. Seamless integration of design and kirchhoff-love shell analysis using analysis-suitable unstructured T-splines. Comput Methods Appl Mech Engrg 2020;360:112765. http://dx.doi.org/10.1016/j.cma.2019.112765.
- [98] Sederberg TW, Zheng J, Bakenov A, Nasri A. T-splines and T-NURCCSs. ACM Trans Graph 2003;22(3):477–84. http://dx.doi.org/10.1145/882262.882295.
- [99] Wei X, Li X, Qian K, Hughes TJR, Zhang YJ, Casquero H. Analysis-suitable unstructured T-splines: Multiple extraordinary points per face. 2021, arXiv preprint arXiv:2103.05726, arXiv:2103.05726.
- [100] Thomas DC, Engvall L, Schmidt S, Tew K, Scott M. U-splines: splines over unstructured meshes. Technical report, Coreform, LLC; 2018.